RADIATION DAMAGE - ELECTRON IMPACT

NASA Research Grant NsG-371

by
F. A. White
D. E. Kraus

Rensselaer Polytechnic Institute
Department of Nuclear Engineering and Science
Troy, New York

Terminal Report
September, 1965

CONTENTS

LIST OF FIGURES

Summary

A theoretical and experimental study was originally proposed to analyse the charge state of recoil ions produced by direct impact from high energy electrons. Theoretical calculations indicated that the intense electron beam currents of the R.P.I. Linac might be sufficient to provide a small number of recoil atoms whose charge state could be determined by a double-focusing mass spectrometer, directly coupled to the Linac drift tube. A lengthy development program resulted in the successful completion of this analyzing apparatus. All efforts to obtain data, however, were unsuccessful and are attributed to the repeated failures of several high-gain ion detectors to recover to a stable operating mode within 10 microseconds after the intense bremsstrahlung burst of the Linac. These and other serious difficulties suggest that this present work should be terminated. This final report makes suggestions relative to any similar future work, although none is anticipated at this time. Although specific objectives of this research study were not achieved, general contributions to the NASA program in pursuit of this work include (1) theoretical calculations of proton induced damage in germanium and silicon (2) a concidence electron and ion detectors for which a NASA patent disclosure was submitted, (3) specialized mass spectrometric equipment that will prove useful in advancing the "state of the art" in low current ion detection, and (4) improvements to general Linac technology.

This study also led to an entirely new concept and proposed method for identifying exceedingly short-lived fission products. An appropriate patent disclosure is in preparation.

Introduction

The original proposal stated that experimental and theoretical work relating to radiation damage seemed to focus on the following areas: (1) the production of displaced atoms and the introduction of imperfections (2) the nature of such imperfections and the effects of annealing (3) correlation of imperfections with the electrical and physical properties of materials. The proposal further suggested that this research attempt focus on the one area in which an insufficient effort was being made, namely, the kinetics of the displaced atoms, per se. The work was proposed in the hope that a correlation could be made to damage, if more specific information could be ascertained relative to charge states, energies, and ranges of the displaced ion centers.

The availability of the R.P.I. Linac using a high energy electron beam seemed to present an advantageous experimental situation compared to neutron bombardment. Radiation damage by neutrons occurs when the neutron interacts directly by collision with the nucleus. The nucleus recoils, taking its electron cloud with it. (The only atomic electrons having an appreciable probability of being stripped from the nucleus are those having orbital velocities less than the nuclear recoil velocity). At low neutron energies this restricts electron stripping to essentially only the outermost electrons, with a low probability of the recoil atom being ionized. The case for electron impact is analogous, with small differences. Prior to the actual experimental efforts, a reasonable probability for obtaining recoil data seemed evident

from (1) the very high density of pulsed electrons available from the R.P.I. Linac, and (2) the long transit time of recoil ions. This latter factor appeared to provide the necessary time interval to discriminate between the detection of a few ions and the intense bremsstrahlung burst generated by the electrons. In retrospect, the difficulty of this discrimination was seriously underestimated.

Theoretical

Theoretical work was initially focused on a correlation of predicted and observed damage in germanium by protons - based on experimentally observed damage in other experiments reported by Dr. J. C. Corelli, et al. Differential cross sections, both elastic and inelastic, have been reported for both germanium and silicon; this effort comprised the Ph.D. research of E. A. Saunders, under the direction of Dr. G. P. Calame.

The specific thesis was titled: "A Calculation of Proton Induced Damage in Germanium and Silicon". This document was made available to NASA-Langley in October 1964. Reproduction of the Abstract only is given below:

"Recent experimental work in the field of high-energy proton irradiation of germanium and silicon (silicon solar cells) has revealed significant deviations between calculated and observed results, particularly for proton energies above about 40 Mev. This work is an attempt to account for the observed results by means of a complete optical-model calculation of elastic and in-

elastic cross sections and the use of the "channeling" theory of Oen and Robinson in the treatment of the displacement cascade. It is known that the reactions which occur in the energy range of concern are predominantly the (p,n), (p,2n) and (p,pn) reactions. However, no satisfactory theory exists for predicting the cross sections for these reactions. Therefore, the Hauser-Feshbach theory for the prediction of (p,p') reactions is used. The resulting reaction cross sections are reduced by a factor more than sufficient to account for the increased Q value of the actual reactions over that of the (p,p') reactions used. The result is an estimate of a lower limit on the number of displacements which can be expected.

Differential cross sections, both elastic and inelastic, are calculated for silicon and germanium for proton energies through 180 Mev and 140 Mev respectively. The cascade model of Oen and Robinson, which takes into account the inhomogeneity of the crystal, is applied to these cross sections to calculate total numbers of displacements in a crystal as a function of the energy of the incident protons.

The results of these calculations of germanium are compared with recently published experimental data obtained using both conductivity and minority carrier lifetime as damage probes. Excellent agreement is obtained using reasonable values of cutoff energy between elastic and inelastic reactions of the primary knockon and of the channeling probability parameter of Oen and Robinson.

Calculated results on silicon are in only fair agreement with available experimental data. The poorest agreement is found for proton energies above 40 Mev. It is concluded that the reduction in mass of the recoiling nuclei resulting from the loss of spallation products is the most likely cause for this discrepancy.

It is concluded that:

(1) the reaction cross sections of both silicon and germanium contribute the dominant portion of the damage observed for proton energies above about 30 to 40 Mev.

(2) cascade models which treat the crystal as a homogeneous mass (e.g., the Kinchin and Pease displacement model) yield results which are in significantly poorer agreement with experiment than are those results using the channeling model of Oen and Robinson.

(3) the damage from proton irradiation on germanium as measured by either change in conductivity or change in minority carrier lifetime is a linear function of the number of displacements, at least through proton energies of 140 Mev.

(4) excellent prediction of damage vs. energy can be obtained for proton irradiation of germanium using a full optical-model calculation and the channeling model of Oen and Robinson.

(5) similar calculations relative to silicon solar cells are not very satisfactory, either because of the increased effect of spallation in silicon or because the damage vs. energy relation for a silicon device is different from that for the material per se."

One conclusion stated in this work (p.125) is specifically pertinent to this work, namely "A most significant contribution to

the solution of the entire radiation-induced displacement problem would be the experimental determination of the charge state of an atom moving in a crystalline solid as a function of the energy of the moving atom. Such a determination is, of course, easier to describe than to accomplish". In retrospect this sentence seems to have special significance.

Questions can be properly raised relative to the precise meaning of data, even if obtained, of recoil ions from a surface (this experiment) as they might apply to charge state inside a crystal. There appeared, however, to be no real alternative.

Initial calculations, performed by Dr. G. P. Calame, were directed to a consideration of estimated counting rates which might be obtained from direct recoils produced by electrons from the R.P.I. Linac, from the surface of a thin target (see Figure 1 and Figure 2).

Consider a 40 Mev electron beam to impinge on a thin target, and to knock an ion out of the target in a direction ϕ_t with the initial beam. The total rate of ions entering the beam in a solid angle w_t about 0_t is desired. This may be found from the equations of relativistic kinematics and from electromagnetic scattering theory.

Let m_e = electron rest mass

p = electron momentum before collision

p_2 = electron momentum after collision

m_t = target rest mass

p_t = target momentum after collision

KE_t = target kinetic energy after collision

E = total energy of electron

Then, as in Rossi (B. Rossi, High Energy Particles, Prentice Hall, New York, 1952, p. 14), the relation between KE_t and θ_t is found to be

$$KE_T = 2m_T c^2 \frac{p^2c^2\cos^2\theta_T}{\left[m_T c^2 + \sqrt{p^2c^2 + m_e^2c^4}\right]^2 - p^2c^2\cos^2\theta_T} \quad (1)$$

The final momentum of the target nucleus is found from

$$p_T c = \sqrt{(KE_T)^2 + 2(KE_T)m_T c^2} \quad (2)$$

The final energy of the electron is

$$E_e = E - (KE)_T \quad (3)$$

The final momentum of the electron is found from

$$p_e c = \sqrt{E_e^2 - m_e^2 c^4} \quad (4)$$

and then the angle of scattering, θ_e, of the electron is found from

$$p_T^2c^2 = p_e^2c^2 + p^2c^2 - 2pp_e c^2\cos\theta_e \quad (5)$$

The cross section $\sigma_t(\theta_t)\, dw_t$ for production of a recoil atom into a solid angle dw_t about θ_t is the same as the cross section $\sigma_s(\theta_e)\, dw_e$ for electron scattering into solid angle dw_e about θ_e. If one uses the Born approximation to compute the latter quantity, one obtains for realtivistic electrons ($\beta \approx 1$), and in the C.M. system,

$$\sigma_s(E_e) = \left\{\frac{Z^2 r_e^2}{4}\left(\frac{m_e c^2}{E}\right)^2 \frac{\cos^2\theta/2}{\sin^4 E_e/2}\left[1 + \frac{\pi Z}{137}\frac{\sin\theta/2(1-\sin\theta/2)}{\cos^2\theta/2}\right]\right\} F^2 \quad (6)$$

where the quantity in the curley brackets is the well known MOTT scattering formula (N.D. Mott, Proc. Roy. Soc. (London) A124, 426, 1929; A135, 429, 1932) as modified by McKinley and Feshback (W.A. McKinley Jr. and H. Feshback, Phys. Rev. 74, 1759, 1948), and F^2 is a "nuclear form factor" which corrects the point charge Mott formula for effects of finite nuclear size (J.H. Smith, Phys. Rev. 95, 271, 1954). While eq. 6 will be poor for heavy elements such as Au, comparison of calculations made from eq. (6) for Cu with exact phase shift calculations show fair agreement at energies of 225 Mev (Yennie, Ranhall, Wilson, Phys. Rev. 95, 500 (1954), so eq. 6 should be reliable at the much lower energy of 40 Mev of interest here. In equation (6), r_e is the classical radius of the electron. With the aid of eqs. (1-6), the necessary computations are easily performed:

A. β for 40 Mev Electrons

$$\frac{m_e c^2}{\sqrt{1-\beta^2}} = 40 \text{ mev}$$

$$m_e c^2 = 0.511 \text{ mev}$$

and β is found to be

$$\beta = 0.99991$$

so the electrons are highly relativistic

B. Recoil Energies of Target Nuclei After Collision

The maximum kinetic energy of a target nucleus occurs when the target recoil angle is $\theta_t = 0$ degrees. Putting $\cos\theta = 1$ in eq. (1), using the excellent approximations

$$m_T c^2 >> m_e c^2$$

$$E >> m_e c^2$$

one obtains

$$(KE_r)^{max} \approx E^2 / E + \tfrac{1}{2} m_r c^2$$

Typical recoil energies are given below:

Target	Maximum Energy
$1H^1$	3.17 Mev
$3L_i^9$	378 Kev
$13Ae^{27}$	127 Kev
$29Cu^{64}$	53.6 Kev

Typical final momenta, found from eq. (2), are

Target	PC
$1H^1$	5903 Mev^2
$3L_i^9$	6340 Mev^2
$13Ae^{27}$	6385 Mev^2
$29Cu^{64}$	6391 Mev^2

It is noted that beyond $3L_i^9$, the final momentum is almost independent of the mass of the target nucleus.

C. Counting Rate for a Thin Target of $29Cu^{64}$* *(Cu-63,65)

Consider a target of $29Cu^{64}$ to be placed in LINAC the electron beam. (See Figure 2) In order not to have the electron beam impinging on the detection apparatus, the angle of ion recoil, θ_t, cannot be zero. We will consider two cases: $\theta_t = 15^\circ$ and $\theta_t = 40^\circ$.

$\theta_t = 15^\circ$ | $\theta_t = 40^\circ$

From (1), we find the energy of the recoil ion

KE = 50.04 Mev | KE = 31.47 Kev

From 2,3,4, we find

P^2c^2 = 5963.2 Mev^2 | P^2c^2 = 3750.2 Mev^2

$E_e = 39.39$ Mev^2	$E_e = 39.97$ Mev^2
$P_e^2c^2 = 1595.74$ Mev^2	$P_e^2c^2 = 1597.34$ Mev^2

Then from (5), the corresponding angle of electron scattering is, using $p^2 C^2 = 1599.74$ Mev^2

$\vartheta_e \approx 150^\circ$	$\theta_e \approx 100^\circ$

It is desired to compute $\sigma_s(\theta e)$. Eq. 6 is for center of mass scattering. A 40 Mev electron has a mass of $\approx 100 m_e$, while the Cu nucleus has a mass of 64(1800) m_e, so the electron mass is $\approx 1/1200$ the mass of the target, and thus the laboratory system differs little from the center of mass system. The angles in eq. (6) are thus approximately the laboratory angles, and using (6), then, the cross sections are

$\sigma_s(150^\circ) = 2.79 \times 10^{-28} F^2 cm^2$	$\sigma_s(100^\circ) = 4.225 \times 10^{-27} F^2 cm^2$

It remains to find the nuclear form factors F^2.

Let $g = \frac{2E}{\hbar C} \sin \frac{\theta e}{2}$ (7)

Where g is the momentum change suffered by the nucleus and $\bar{r}$ the root mean square radius of the nuclear charge distribution. Using $\frac{\hbar C}{2} = 1.581 \times 10^{-11}$ mev-cm, g for the two cases is

$g = 2.54 \times 10^{12}$ cm^{-1}	$g = 2.01 \times 10^{12}$ cm^{-1}

If the nucleus is regarded as a uniform charge distirbution of radius R, then the root mean square radius is $\bar{r} = R\sqrt{\frac{3}{5}}$. Using data from table IV of Hofstadter's work (R. Hofstadter, Rev. Mod. Phys. 28, 214, 1956), choose R as ≈ 5.00 Fermis, whence

$g\bar{r} = .985$	$g\bar{r} = .780$

and then from model II is figure 4 of Hofstadter's paper (loco. cit.), F^2 for both cases is approximately .7.

Finally then

$$\sigma_s(150^\circ) = 1.95 \times 10^{-28} \text{ cm}^2 = \sigma_r(15^\circ) \qquad \sigma_s(100^\circ) = 2.96 \times 10^{-27} \text{ cm}^2 = \sigma_r(40^\circ)$$

If the target is considered to be an atomic monolayer of Cu, then the monolayer contains approximately 1.89×10^{15} atoms/cm^2. If the LINAC is operated with a 4.5 μ sec pulse width of average current .5 amps at a repetition rate of 60 cycles, then the target is being bombarded with $.844 \times 10^{15}$ electrons per second. The number of target atoms scattered into a unit solid angle $d\omega$ about the angle in question is then, in the two cases

$3.11 \times 10^2 d\omega_r$ particles/sec $\qquad$ $4.72 \times 10^3 d\omega_r$ particles/sec

If the acceptance angle in θ_t is 2°, and the azimuthal acceptance angle is denoted by $d\phi_r$, then in the two cases

$$d\omega_r = .0085\, d\phi_r \qquad d\omega_r = .0224\, d\phi_r$$

and the counting rates are then

$2.64\, d\phi_r$ counts/sec $\qquad$ $106\, d\phi_r$ counts/sec

The predicted counting rates thus suggested that an experiment involving the detection of recoil target nucleus might be possible for small scattering angles only if the azimuthal acceptance angle is made large. However, for a large θ_t (40°) a small azimuthal angle is allowed (see also Appendix I).

Experimental Developments

Although it was a major disappointment to encounter failure to obtain significant data, a larger effort was made experimentally than was originally proposed. Initially a double-focusing mass spectrometer was suggested to analyze any recoil ions having any charge state. Not only was this unit built, but two additional major projects were programmed and completed, (1) a time-of-flight spectrometer, and (2) a coincidence detector for high energy ions. All three of these developments will be reviewed in consideration of the exceedingly large investments of time by the authors in these projects - and their possible value to future investigators.

A. Double-Focusing Mass Spectrometer

A double focusing system of large radius was selected to achieve:

1. Collection of ions having a large energy spread.
2. Reasonable transit time from ion production to detector (to minimize bremsstrahlung effect).
3. Energy and momentum analysis.
4. Charge state analysis.

A plan view of this instrument is shown in the scale drawing schematic of Figure 3.

Considering only the monolayer of atoms which recoil from the far surface of a foil, these atoms should escape without energy degredation. The electrostatic analyzer provides charge identification for a cylindrical lens ($R = 2\ V/n\bar{E}$) where R is the radius in

centimeters and $\overline{E}$ is the electrostatic strength of the lens, and n is the effective charge of the ion. Thus for a given radius (fixed), the charge state of the ion can be determined if its kinetic energy is known, or the K.E. of the particle can be determined if the charge state is known. It will be noted that this relationship is mass independent, and that the voltages across the plates of the lens for a multiply charged ion will be 1/n times that required for a singly charged atom. The lens was designed to accept singly charged recoil atoms up to a maximum of 60 Kev. For the particular spacing selected, this corresponded to 10,000 volts on both positive and negative electrostatic plates.

A radius of 20 inches was selected to correspond to that of the magnetic analyzer.

The pair of cylindrical lenses were machined from stainless steel forgings, suitably annealed (see Figure 4). "Stand-off" insulators were made from special billets of alumina whose expansion coefficient was precisely measured in the G.E. Research Laboratory in Schenectady. After machining in the R.P.I. shops, these were "fired in the Metals and Ceramics Laboratory of G.E. These ceramics had a low vapor pressure and showed no signs of voltage breakdown or current leakage after many months in the Linac target room.

Two "Z" focusing or "einzel" lenses were designed to achieve some degree of strong focusing in the vertical plane, (see Figure 5).

The electromagnet was selected to be 90^{o}-20"R for several reasons. These included (a) reasonably long flight path (b) compact geometry of magnet assembly, and (c) ability to focus ions over a

very large energy range. It was clear at the outset that cost limitations would preclude the purchase of such a magnet from commercial sources. Hence a significant amount of effort was directed to engineering and design details. The final unit, complete with exciting coils, totaled approximately 5 tons. The machining of the magnetic yoke was contracted to the Allen Tool Co., Syracuse, New York. The exciting coils were manufactured by the transformer shop of the General Electric Co., Schenectady, New York.

The general configuration of the magnet can be noted in the photograph of the completed electromagnet (Figure 6). A "C" shaped yoke is fabricated from 8-inch thick plates of low carbon steel. A pair of exciting coils surround a central core which is mated to the 90°-20-inch mean radius pole pieces. In order to accommodate a widely diverging beam the peripheral radii of the pole pieces are 22.5" and 16.5". The pole gap is 1.035 inches.

An advantageous feature of this magnet design is that the unit can be operated at high flux densities without water-cooling. It has also been designed to operate from inexpensive, low-current, commercially available power supplies. Each coil is comprised of approximately 11,600 turns of 0.054" diameter, heavy formex-covered copper wire. The mean length per turn is 7.3 ft; total weight per coil is approximately 750 lbs; total resistance per coil is about 300 ohms. When the pair of coils is connected in parallel to a 300 volt-2 ampere power supply, the magnet can be programmed over an exceedingly wide range of fields. At an exciting coil current of only 1.0 amperes per coil the magnetic field attained in the gap is 9,750 gauss. The approximation to linearity from exciting coil

current is shown in Figures 7a and 7b.

Clearly, this magnet appears to be entirely satisfactory for the analysis of very high energy recoil ions. Below are indicated the maximum energy of singly charged atoms which could be analyzed at maximum magnetic field (9,750 gauss):

Recoil Atom	E (maximum)
H^1	11.8 Mev
He^4	2.95 Mev
Al^{27}	425 Kev
Cu^{63}	188 kev
U^{235}	51 Kev

Higher charge state particles can, of course, be analyzed with decreased magnetic fields (see Figure 8). Thus, the magnet appears to be satisfactory for much higher energy ions than were anticipated in the present work. The conservative design, however, insures greater experimental flexibility. For example, the lower pole piece is removable; it can be replaced to provide a 2" rather than a 1" gap at reduced field - if, a larger gap is needed at some future date to improve the ion counting rate.

The main vacuum housing of the spectrometer met every specification. A 75 liter ion-pump achieved a pressure of 1×10^{-7} mm. The detector end of the analyzer was independently pumped by a 15 liter unit. In initial tests, prior to assembly on the Linac:

(a) ultimate vacuum measured 8×10^{-8} mm Hg

(b) Cs-133; Rb-85,87; K-39, Na-23, and Li6,7 were observed. A 10 Kev - 20 Kev ion gun was used.

(c) "Z" focusing effectively enhanced the collection efficiency.

A scale drawing (front elevation) of the vacuum chamber assembly is shown in Figure 9.

The 20" radius mass spectrometer magnet was placed in the R.P.I. Linac Target Room in July 1964 and the other components were installed in August. The double-focusing instrument was positioned with its source focal point on the central drift pipe of the Linac - approximately 70 feet from the last section of the accelerator. Electron beams of 700 milli-amperes with an energy spread of 8% full width at half-maximum were delivered to a 2 centimeter circle at this point.

Figure 10 shows the connection of the source chamber to the drift tube with isolation vacuum valves, the stainless steel electrostatic analyzer housing, the transition section containing a "Z" focus lens and vacuum pump manifold, and the 5-ton electromagnet. Figure 11 shows a section along the drift pipe, and the detector housing for the two-twenty stage multipliers. The installation proved compatable with existing vacuum facilities, and did not interfere with the use of the accelerator target stations beyond it. Differential pumping using 0.0003 inch aluminum foil permitted vacuum of 10^{-7} mm to be maintained within the spectrometer, (pressure is 5×10^{-6} mm in drift sections) while the beam is being passed through the recoil chamber.

A removable electron beam drift pipe extension and water-cooled aluminum beam-stopper, were constructed and installed for

use during preliminary testing, in order to minimize penetrating radiations at the detector during beam stopping. (Figure 12 shows the beam stopper in the concrete cavity at the end of the Target Room).

All electrical parameters of the spectrometer were remotely programmed and could be changed without interruption of accelerator operation.

The recoil box held 3 foil samples to be tested without breaking vacuum, and includes an ion test source for the spectrometer. A surface ionization type source, using Cs-133 as the accelerated ion beam, was employed to determine the efficiency of the double-focusing system to simulate recoil ions having a wide energy spread. Results of a single test are displayed in Figure 13. It will be noted that the spectrometer can transmit a large fraction of ions produced in the source region, even though the spread in their kinetic energies is several per cent. This feature is a prerequisite for detecting recoil atoms from any target when the spectrum of recoil atoms originate from many monolayers.

An outline of the basic ion optics problem is given in Appendix II.

Time-of-Flight Spectrometer

As soon as there was evidence that the radiation background might be of such severity as to preclude obtaining significant data in the double focusing system, a decision was made to supplement this analyzer by a simple time-of-flight tube. Accordingly a 3.5 meter tube was built which provided for (a) independent ion pumping

(b) an orientation identical to the other spectrometer, i.e., 45^{o} angle of recoil (c) wide angle ion detector, (d) a thick window for insertion or removal in the flight path, and (e) provision for electrostatic or magnetic filtering, not analyzing.

Because of the marginal nature of the experiment, it was believed that this extra device would complement the original apparatus in the following respects:

1. The detection of all charge-stages (including neutrals) and energies during a single run.

2. The possibility of determining the ratio of neutral to charge ions as a function of recoil energy.

3. Independent prompt determination of accelerator energy, recoil by foreign surface atoms, and energy degration of recoils by foreign surface layers.

4. Rough determination of absolute cross sections, since electron beam current, recoil trajectory, and detector efficiency might be known to about 10%.

5. Subsequent inclusion of a crossed-field filter with time dependent electrostatic field on the time-of-flight leg would enable the determination of individual charge states.

The two physical schemes are shown in Figures 9 and 10. The first unit was made of aluminum, the second was made of stainless steel with a two vacuum interlocks and a duraluminum chamber for housing the detector. (An independent check of the detector optics is given in Appendix IV) Figure 15 is a photo of the time-of-flight tube and Figure 16 is one model of the wide solid angle "converter foil" and electron multiplier. Figures 17 and 18

respectively indicate ion energies and ion flight times (for approximately 3 meters) in ion-electron kinematics.

Development of Coincidence Detector

Perhaps the most profitable by-product of this ion-recoil effort is the conception and development of a scheme which has the potential for many applications by other investigators.

This invention relates to a system for detecting single electrons, ions or neutral atoms. It makes possible a discrimination against usual source of "noise" such as unwanted thermionic electrons in photomultiplier tubes, and it permits the detection of a very small number of particles, even in high radiation environments. A formal patent disclosure has been titled "Secondary Emission Coincidence Scheme of High Sensitivity for the Detection of Single Electrons, Ions, and Other Particles". The disclosure was dated January 15, 1965, in a letter to Dr. Smull, by F. A. White, citing F. A. White and D. E. Kraus as co-inventors.

The basic scheme is made clear by reference to Figure 19. The coincidence multiplier is comprised of (1) a particle "converter" (2) an electron focusing system (3) two electron multipliers and (4) a coincidence circuit.

It is known that high gain electron multiplier can be employed to detect photons (with a photo-cathode to convert light to electrons) or single charged particles. An important limitation, however, is the fact that a few electrons are usually emitted from the first cathode or succeeding "dynodes" at room temperature. These "background" electrons limit the ultimate particle sensitivity that

can be achieved. It is difficult, for example, to detect currents of less than one electronic charge per second (1.6×10^{-19} ampere) due to this and other factors. Furthermore, these devices have a marked increase in "background" current if these are utilized in radiation fields which produce secondary electrons on any or all the multiplier dynodes or electron amplifying surfaces.

In this invention, both of these limitations are substantially bypassed by causing an electron or positive ion to penetrate the "converter" rather than terminate its trajectory in a conventional multiplier detector. Consider a 500 A^{o} foil which is sufficiently thin so that an electron of a few thousand volts kinetic energy or a light ion, for example, Li-6, 0.16, Na-23 of $\sim$ 30 Kev) can penetrate this foil. The ion, if it penetrates the converter, will cause the emission of one or several secondary electrons from the front surface of the converter. It will also, however, give rise to the production of secondary electrons as it leaves the back surface of the converter, even if it emerges as a neutral atom rather than an ion. Providing only that the residual kinetic energy is sufficient to generate one or more secondary electrons, we now have the advantage of detecting <u>two</u> simultaneous bursts of secondary ejected electrons generated from a <u>single</u> particle.

The converter thus generates two groups of secondary electrons of very low kinetic energy (a few electron volts). These groups of electrons, on opposite faces of the converter, can easily be focused by conventional electron optics onto the first cathode or dynode of high gain multipliers. Output pulses from both of these

multipliers can be fed into a coincidence circuit which will trigger only when simultaneous signals arise in the multipliers.

The advantages of this scheme are significant for the detection of particles or groups of photons which can be caused to generate simultaneous secondary electrons on each side of such a "converter foil" or target. These include:

1. The detection of an exceedingly small number of events per unit time, and the freedom from thermionic "noise" over a greatly extended time interval. (For example, in "conventional" photomultiplier tubes a background or "dark" current of 10^{-18} amperes is considered good. With this coincidence scheme, an "effective" background current can be reduced by a factor of 10^{5}, to 10^{-23} ampere. This implies that suitable particles can be detected in the range of one even per hour.

2. Discrimination from spurious pulses generated from the secondary electronic production of the many dynodes of a single multiplier in a radiation environment. Shielding requirements can then be minimized or eliminated.

3. Directional discrimination.

4. Wide area collection.

5. Fast response - generally better than a fluorescent material used in a coincidence arrangement.

A prototype detector has been construced and tested. Two models, in fact, have been built. The second operated successfully and was tested as follows:

1. Electrons - A current estimated to be 10^{-16} ampere was made to impinge upon a 500 A^{o} nickel "converter" and coincidence

multiplier scheme. Pulses, coincident within 5 x 10^{-8} second were observed on both multipliers. When observed with a fast oscilloscope, no random or thermonically emitted electrons were observed in coincidence. Figure 20 shows the approximate minimum energies required for primary electrons to penetrate several foil materials. (Ref. C. Feldman, Phys. Rev.117, 455 (1960)) At 3000 eV coincidence pulses were observed.

2. Positive ions - Lithium atoms were focused on the converter. At 30 Kev, coincident pulses were observed. Ion currents were approximately the same as electron currents in this test. A one to one correspondence was not observed, but it is believed that a thinner foil would have given better results because the heavy ions have a small range, and heavier atoms - Na-23, K-39, Cs-133 may have been impurity ions in the unresolved beam. (See Figure 21 and 22.)

3. Gamma Rays - The device was tested by gamma rays from a Po-Be radioactive source, rated at 11.5 mr at one meter. At 10 centimeters from this source no coincident gammas were observed.

4. Photons - Photons, emitted randomly, from a hot filament, produced secondary electrons (and hence output pulses) from both multipliers. The photon intensity could not be estimated, but with high counting rates in either channel ($\sim$105/sec) no coincident output pulses were observed. Both this and Test #3 prove the performance of such a scheme against "background" events.

Slight modification of the principle of the scheme makes possible detection of other radiations (neutrons, and alpha particles in the presence of high backgrounds). The converter

foil would be replaced with material sensitive to these radiations (e.g. B^{10}, Li^{7} for neutrons) sufficiently thin that the range of particles produced in this interaction would reach both converter surfaces. (Figures 23 and 24 show two coincidence assemblies.)

More complex geometries would permit secondary electrons produced on the same side of the converter material, but having different initial directions of motion, to drift into opposite multiplier geometries.

Improvements Relating to Reactor Technology

Several developments in the course of this work merit mention. There are of the type which seldom appear in the technical literature but they are the result of the specific experience gained in this attempted investigation. These include:

A. Isolation of the Linac Vacuum by Thin Foils

Early in the experiment it was deemed necessary to isolate the flight path of ions (in the spectrometer) from the Linac drift pipe. The problem was to allow electrons to interact directly with ions, but maintain a higher vacuum (10^{-7} mm) in the spectrometer, compared to the drift pipe of the Linac (10^{-5} to 10^{-6} mm). A solution proved to be the use of a pair of very thin Al foils (0.3 mil thick), 1½" diameter, placed along the drift pipe at juncture of the spectrometer. Their location was before, and beyond, the ion recoil sample foil. This pair of foils effectively allowed exceedingly good differential pumping in the spectrometer and provided high vacuum even with poor vacuum in the Linac drift section. The foils also restrained back-streaming of vapors from

the accelerator's diffusion pumps. Important was the fact that these foils generated little electron scatter at 40 Mev and needed no water cooling even when the Linac was operated at full power.

B. Use of Ion Pumps for the Linac

The very successful operation of Vac-Ion pumps for the spectrometer ultimately led to adapting ion-getter pumps for entire Linac operation. Power control units, of course, were operated outside of the radiation target area. The electron gun of the Linac is especially susceptable to vacuum failure, oil backstreaming, etc., and this experiment pointed to the desirability of this major change in the entire Linac vacuum system. Currently the Linac is completely ion pumped - from injector to target.

C. Operation of Solid State Devices in a High Radiation Environment

A block diagram for a portion of the electronic circuitry is shown in Appendix IV. It is of interest to note that a discriminator built to accept pulses from the electron multiplier was unconventional in the sense the solid state devices were used in a high radiation environment. A Philco 2N501 transistor survived a month of irradiation at average levels of about 20 R/hr with peak irradiations of about 10^5 R/hr when operated. General performance appeared unimparied.

D. Use of Indium Wire as a General Vacuum Seal Material

Indium wire (0.050 and .080 diameters) was used as the metal-to-metal seal for all major joints in connecting the vacuum chamber parts. It was simply laid on the rough ground joints which were

then bolted together by stainless steel bolts. No gasket groves were required, finish grinding or polishing was unnecessary and the vacuum seals proved tight for 10^{-8} mm pressure for about 1 year. When compressed the wire assumed the shape of thin ribbons or foils about 2-3 mils in thickness. The technique is cheaper than using gold foils or wires, and there is no restriction as to the shape of the mating surfaces.

Program to Obtain Experimental Data

Because of the failure to obtain significant data, this terminal report can only review the difficulties and comment on any anticipated efforts by future investigators ccmtemplating similar work. Most of the experimental features of the apparatus have been described in previous pages and supplemented by appropriate figures.

A large fraction of Linac operational time was expended unprofitably. After initial experiments, it became clear that several facets of this investigation required detailed studies relating to ion optics, electron multiplier efficiencies, analysis of electron and recoil ion energy spread. Several demands are placed on the Linac to provide electrons which are close to a single energy --- at high currents. Figures 25 and 26 indicate about the best performance at high currents. The need for monoenergetic electrons is emphasized by the fact that the spread in recoil ion energies will depend on E^2.

A much more crucial difficulty, not envisioned in the design of this experiment, was that an exceedingly high radiation background persists in the Linac target area ---- many tens of microseconds after the primary intense bremsstrahlung. The prompt bremsstrahlung was not the general source of difficulty, although this gave rise to detector saturation which prevented detection of light ions with short transit times. The background which could not be overcome, however, is attributed to a reasonably large flux of slow neutrons which eventually give rise to capture gammas that generate spurious counts in the detector. After many months of

effort, this difficulty eventually led to an attempt to detect low energy neutral atoms of a heavy element - (Au-198), in the hope that recoil atoms of gold, even undergraded in energy, might be observed because of their long transit time. Gold also appeared desirable, as it is presumed to have a minimum of surface impurities.

Reference is made to Figures 27, 28, and 29 as exemplary of large output of data which failed to yield fruitful results because of this background limitation. It should be noted that all three graphs correspond to output counts resulting from 100,000 Linac bursts in the time-of-flight spectrometer. The data exhibited in Figures 27 and 28 were taken at an electron multiplier voltage of 6,400 V, at which setting the detector discriminator level was believed to respond efficiently to a single secondary electron spectrum from the "converter" foil. The data for aluminum of two thick masses appear to indicate a component of background corresponding to intervals greater than 50 microseconds, that is proportional to the number of atoms in the electron beam. No mechanism for this component has been demonstrated.

The data of Figure 28 shows a pulse spectrum in time slightly later than the time-of-flight for elastic recoils, and persists to times corresponding to gold ion energies of about 300 eV. Such a spectrum might be produced by the surface flux of the ion cascade when weighted by the detector sensitivity as a function of energy.

Data taken at an electron multiplier voltage of 5900 V, where the single-electron spectrum, and hence the low energy ions are more strongly discriminated against, are shown in Figure 29. Here

a large number of events occur before the arrival of the undergraded elastic recoils. The indicated conjecture has no confirmation save the rough agreement with energies expected in such a process.

One of the more important experimental tests run in 1964 was the mass spectrometric detection of Cesium-133 atoms in the time interval between Linac bursts. The success of this early test led to considerable optimism as an electron multiplier with Be-Cu dynodes appeared to recover promptly and gave no evidence of a change in ion detection efficiency. Subsequent multipliers were constructed of aluminum (to prevent activation), and this change may be a poor one. Although Allen-type electron multipliers made from aluminum were successfully tested, they did not appear to have the stability of the Be-Cu alloy type.

Tests subsequent to the data displayed in Figures 27 - 29 were made with a "normalization" (see Figure 30) for efficiency of multipliers - as they appeared to operate as a function of time, for intervals many microseconds after a burst. Thus no direct evidence can be unambiguously presented in support of ion recoil phenomena for either neutrals or charged particles. It is difficult to avoid the conclusion that either most of the recoils do not reach the detector or that the detector efficiency following the beam burst is so poor that probability of detection is drastically reduced. Physical mechanisms for the first possibility are review in the Appendix and none of these considered is found sufficient to produce such an effect.

Conclusion

1. The original technical argument for this experiment - that

radiation damage is significantly affected by the charge state of the recoil - has no firm theoretical ground in the region below ionization cutoff. Three contentions remain which argue for an attempt to perform an experiment of this sort.

a) The experimental techniques required are probably more easily developed at the lower recoil energies below ionization cutoff.

b) The idea of an ionization cutoff is an abstraction, of limited value in quantitative calculations intended to choose among theoretical alternatives. It is possible, although hardly certain, that an examination of the charge state distribution in the energy range approaching nominal cutoff values would reveal features tending to sharpen the idea of an ionization cutoff.

c) Examination of the surface flux in energy and charge state should reveal something of the mean collision interval and the charge state as a function of energy in a cascade process.

2. The experimental techniques required for this experiment have not been developed even for lower recoil energies.

a) Electron multipliers and associated gating techniques are apparently inadequate. Future design should consider extensive examination of secondary emission surfaces under heavy radiation, efforts to reduce the size of the multiplier structure, the possibility of pulsing the entire dynode chain, the positioning of gating elements in a multiplier structure, and the use of time-dependent ion optics to reduce the sensitive area of converter required.

b) The large gains required of detector structures operating in environments with high electrical noise make them particularily vulnerable to the overload phenomena observed. Practical

discrimination levels for this experiment are about 10^7 electrons. It is reasonable to entertain the hope of discriminating at levels an order of magnitude lower, if tunnel diode stripline structures are at the collector inside the multiplier vacuum envelope.

c) The background at times greater than 20 usec aside from that arising within the multiplier itself, can be reasonably ascribed to conversion of γ's from (n,γ) reactions within the room. Those arising from deuteron formation have energies requiring several inches of steel, which has a small photo reaction cross-section, and will not sustain a further neutron-photon cascade.

d) An alternative scheme is to "pipe" the ions effectively to a remote location outside the Linac target room, or provide a "block house" within the target room area; this scheme will not work for neutrals.

3. Any future experiment should be planned to include variation of recoil angle.

4. As indicated in the Summary, although specific objectives were not achieved, useful contributions included (a) theoretical calculations (b) a coincidence scheme for ion or electron detection (c) specialized mass spectrometric equipment, and (4) improvements to general Linac technology. It also seems clear that, at some future date, the precise measurement of ion recoil energies may be usefully employed to accurately measure primary electron beam energies.

5. A recommendation has been made to utilize the apparatus developed in this effort to support of other NASA related studies in mass spectrometry.

ADDENDA

A Method for Determining Fission Products Having Exceedingly Short Half-Lives

Abstract

A novel experimental method is proposed which permits the identification of nuclides produced by fission induced by high energy electrons and gamma rays. Whereas fission products, in the general case, can be identified if their half-lives of decay are greater than one second, this invention suggests a technique that allows the isotopic identification of fission products having life times in the 10^{-3} to 1 second range. The basic scheme involves (1) production of fission products by a Linac in a thin filament impregnated with fissile material, (2) prompt thermal diffusion of fission products in this filament by operating it at a high temperature, (3) fission product ionization by surface ionization of this same, or auxiliary filament, and (4) mass analysis of fission products in a double focusing spectrometer. (see Figure 32)

Advantages over other methods include a favorable geometry for collection and mass resolution within a single mass unit.

A separate communication, to document this concept, will be forwarded to NASA.

APPENDIX I

Cross-Section for an Elastic Scattering Process

The cross-sections for an elastic scattering process at 40 Mev will fall between 10^{-26} and 10^{-27} cm^2/steredian for Ag, Au, Ni, and Cu, the lower form factor for large Z roughly balancing the Z^2 factor in this region. The estimated count rate then becomes

$$R = E \frac{d\sigma}{d\Omega} \Delta\Omega N_A \cdot N_e \cdot L$$

where $E \sim 0.3$ = detector efficiency

$\frac{d\sigma}{d\Omega} \sim 3 \times 10^{-27}$ = cross section

$\Delta\Omega \sim 10^{-4}$ = solid angle

$N_A \sim 10^{15}$ = atoms/monolayer

$N_e \sim 2 \times 10^{12}$ electrons in an 0.4 μs, 1 ampere burst

$L \sim 5$ = an estimate of the number of layers furnishing undergraded recoils

$R \sim 10^{-3}$ detected recoils per burst.

In addition to these recoils, which should be detected in a time interval approximately $\Delta T = .02\ T$ where T is the Time of flight ($\Delta T \sim 0.7\ \mu s$, $T \sim 35\ \mu s$ for gold at 40 Mev), the cascade produced recoils degraded in energy should appear in subsequent time channels, and that fraction which is charged should be detected with uniform efficiency because of the post acceleration.

Van Lint et al find approximately half the recoiling nuclei from (γ ,n) reactions on copper under irradiation by 30 Mev and point bremsstrahlung.

APPENDIX II

Ion Optics

The first crder matrices for the 20" double focusing mass spectrometer are given on the accompanying page, together with the locations and dimensions of the stops.

A few additional remarks enable us to estimate the solid angle subtended by the spectrometer.

Momentum and angle are connected by the kinematics of the recoil process to good approximation as

$$\frac{\Delta p}{p} = \frac{\sin\theta}{\cos\theta}\, d\theta = -d\theta, \quad @\ \theta = 45^\circ$$

the initial vectors are thus limited to:

$$\begin{pmatrix} \Delta x \\ \Delta\theta \\ -\Delta\theta \end{pmatrix}$$

for undergraded recoils. In the Z-direction the volume of phase space which can be matched to the magnet vacuum envelop is that contained within phase space region: $(0.75 \times \frac{0.75}{35})$ inch-radians as it is unlikely that the electron beam spot size can be brought to the spectrometer axis with a precision greater than 0.375". Liouville's theorem requires that the largest angle which a perfectly designed lens system can subtend in the Z-direction is $\frac{0.75}{35} \times \frac{0.75}{0.375} = \frac{1.5}{35}$ radians. Direct calculation of the field strengths required to secure such an optical system with lenses of the design and location employed shows, however, that the subtended angle in practice will be much closer to the $\frac{0.75}{100}$ defined by the exit port of magnet vacuum envelope.

The principal stop in the horizontal plane occurs about midway through the magnet vacuum envelope, and limits transmission

to $^{+\ .03}_{-\ .04}$ = .07 radians.

The acceptance angle of the spectrometer is then about 5 x 10^{-4} steradians provided lateral displacement of the beam spot is held to less than 0.25 inch.

$$\begin{bmatrix} 1 & L_3 & 0 \\ 0 & 1 & 0 \\ 0 & 0 & 1 \end{bmatrix} \begin{bmatrix} \cos\theta & R\sin\theta & R(1-\cos\theta) \\ -\frac{\sin\theta}{R} & \cos\theta & \sin\theta \\ 0 & 0 & 1 \end{bmatrix} \begin{bmatrix} 1 & L_2 & 0 \\ 0 & 1 & 0 \\ 0 & 0 & 1 \end{bmatrix} \begin{bmatrix} \cos 2\Omega & \frac{R}{2}\sin 2\Omega & \frac{R}{2}(1-\cos 2\Omega) \\ -\frac{2\sin 2\Omega}{R} & \cos 2\Omega & \sin 2\Omega \\ 0 & 0 & 1 \end{bmatrix} \begin{bmatrix} 1 & L_1 & 0 \\ 0 & 1 & 0 \\ 0 & 0 & 1 \end{bmatrix}$$

L_3: $L_3 = 20''$ — M: $R = 20''$, $\theta = 90°$ — L_2: $L_2 = 27''$ — E: $R = 20''$, $\Omega = 90°$ — L_1: $L_1 = 7''$

$$\begin{bmatrix} 1 & 20 & 0 \\ 0 & 1 & 0 \\ 0 & 0 & 1 \end{bmatrix} \begin{bmatrix} 0 & 20 & 20 \\ -.05 & 0 & 1 \\ 0 & 0 & 1 \end{bmatrix} \begin{bmatrix} 1 & 27 & 0 \\ 0 & 1 & 0 \\ 0 & 0 & 1 \end{bmatrix} \begin{bmatrix} -.606 & 11.26 & 22.2 \\ -.05627 & -.606 & .795 \\ 0 & 0 & 1 \end{bmatrix} \begin{bmatrix} 1 & 7 & 0 \\ 0 & 1 & 0 \\ 0 & 0 & 1 \end{bmatrix}$$

STOPS: +2.0 −2.5 | +2.0 −2.5 | ±0.625 | ±0.625

$$\begin{bmatrix} 1.000 \end{bmatrix} \quad \begin{bmatrix} -1.125 \\ .1062 \\ 0 \end{bmatrix} \quad \begin{bmatrix} -2.125 \\ -.0563 \\ 0 \end{bmatrix} \quad \begin{bmatrix} -.606 \\ -.0563 \\ 0 \end{bmatrix} \quad \begin{bmatrix} 1 \\ 0 \\ 0 \end{bmatrix} \quad \begin{bmatrix} 1 \\ 0 \\ 0 \end{bmatrix} \begin{matrix} \Delta\chi \\ \chi' \\ \Delta\rho/\rho_0 \end{matrix}$$

$$\begin{bmatrix} 0 \\ 0.010 \\ 0 \end{bmatrix} \quad \begin{bmatrix} -.200 \\ +0.010 \\ 0 \end{bmatrix} \quad -.2828 \quad \begin{bmatrix} -0.200 \\ -0.010 \\ 0 \end{bmatrix} \quad \begin{bmatrix} .0702 \\ -.0100 \\ 0 \end{bmatrix} \quad \begin{bmatrix} .07 \\ .01 \\ 0 \end{bmatrix} \quad \begin{bmatrix} 0 \\ .01 \\ 0 \end{bmatrix}$$

$$\begin{bmatrix} .0006 \\ -.02117 \\ .01 \end{bmatrix} \quad \begin{bmatrix} .300 \\ -.0149 \\ .01 \end{bmatrix} \quad .388 \quad \begin{bmatrix} .441 \\ .00795 \\ .01 \end{bmatrix} \quad \begin{bmatrix} 0.222 \\ .00795 \\ .01 \end{bmatrix} \quad \begin{bmatrix} 0 \\ 0 \\ .01 \end{bmatrix} \quad \begin{bmatrix} 0 \\ 0 \\ .01 \end{bmatrix}$$

$$\begin{bmatrix} -.500 \\ +.0249 \\ -.01 \end{bmatrix} \quad -.67 \quad \begin{bmatrix} -.641 \\ -.01795 \\ -.01 \end{bmatrix} \quad \begin{bmatrix} -.150 \\ -.01795 \\ -.01 \end{bmatrix} \quad \begin{bmatrix} .07 \\ .01 \\ -.01 \end{bmatrix} \quad \begin{bmatrix} 0 \\ .01 \\ -.01 \end{bmatrix}$$

HORIZONTAL TRANSFER MATRICES
LENGTH UNIT: INCH
ANGLE UNIT: RADIAN

APPENDIX III

Interference Mechanisms

Electromagnetic

The impulse delivered to an ion in charge state, Z, by a single electron packet (about 20° out of 360° at a frequency of 13000 mc) is, assuming peak current of 1 ampere is

$$\Delta p = \frac{Q z e^2}{c b} \qquad \text{(dyne-sec)}$$

where $Q \sim 10^6$ electrons

$c = 3 \times 10^{10}$ cm/sec

$e = 4.8 \times 10^{-10}$ esu

$b \sim 0.1$ cm

$$= \frac{10^6 \times 2.5 \times 10^{-19}}{3 \times 10^{10} \times 10^{-1}} \sim 10^{-22} \ \frac{\text{(dyne-sec)}}{\text{unit charge}}$$

p for a representative recoil might be:

$$\sqrt{10^4 \text{ ev} \times 1.6 \times 10^{-12} \ 2 \cdot \frac{100}{6 \times 10^{23}}}$$

$$= \sqrt{10^{29} \quad 3 \times 10^{-15}} \text{ (dyne sec)}$$

The thousand or so packets in a single machine burst should not perturb momentum by more than

$$\frac{\Delta p}{p} = \frac{2 \ 10^{-19}}{3 \times 10^{-15}} = 2 \cdot 0.003\% \text{ thermal.}$$

Energy deposition in a thin foil can lead to high local temperatures during the electron burst. This may, because of the thermonic emission, give rise to electron depleted regions at the surface of the foil. It may also cause a large number of surface

layer atoms to be evaporated. Neither consideration explains the absence of observable count rate on the time-of-flight leg. The presence of an electron cloud might increase the proportion of neutral recoils.

APPENDIX IV

Determination of Detection Efficiency

The scheme for determining detector gain and efficiency is shown in Figure 31. A beam of cesium ions is directed into the electron optics and measured by picommeter; the current is adjusted to 10^{-12} amps a pinhole shutter is then placed in the beam, its attenuation ratio having been determined at higher currents to be about 1:500. The beam of 5×10^{-14} should then give count rates of about 3×10^{5}/sec at 100% efficiency.

The pulses may also be sent to a charge-sensitive preamplifier sorted by pulse height. The median gain and width of the pulse height distribution may then be found.

The ion source may be tilted by about 5^{o} around horizontal and vertical to estimate the relative efficiency of the detector as a function of beam incidence position.

At count rates of 10^{5}/sec median gain could be stabilized above 2×10^{7} for observations of about 1 hour. This was an acceptable discrimination level for the electronics relative pulse height distribution is shown in Figure 33. Efficiency under these conditions was about 0.5. At the center of the converter foil relative efficiency between center and regions about 1" from center was about 1.6. Overall absolute efficiency was estimated at 0.35.

1) The aluminum dynode multipliers have several undesirable characteristics.

Their gain deteriorates rapidly with increasing count rate, and also falls slowly at fixed count rate; both effects are observable at rates as small as 1000 c/sec. Both effects are

partially reversed by removing high voltage from the dynode chain for several minutes

2) Extremely high multiplier pulse rates (such as those experienced during the under bremsstrahlung irradiation in the Linac target room) will induce an anomalous increase in the noise pulse rate from the multiplier for several hundred microseconds following the flash. This effect which has a number of puzzling features.

In continuous hard service - several days of experimental running an aluminum multiplier gain will undergo a slow steady deterioration of a factor of ten or more. These observations are probably complicated by the poor pressure ($\sim 5 \times 10^{-6}$ min) which varies with filament current and with multiplier gain. The unwise choice of cesium as an ion further confuses interpretation.

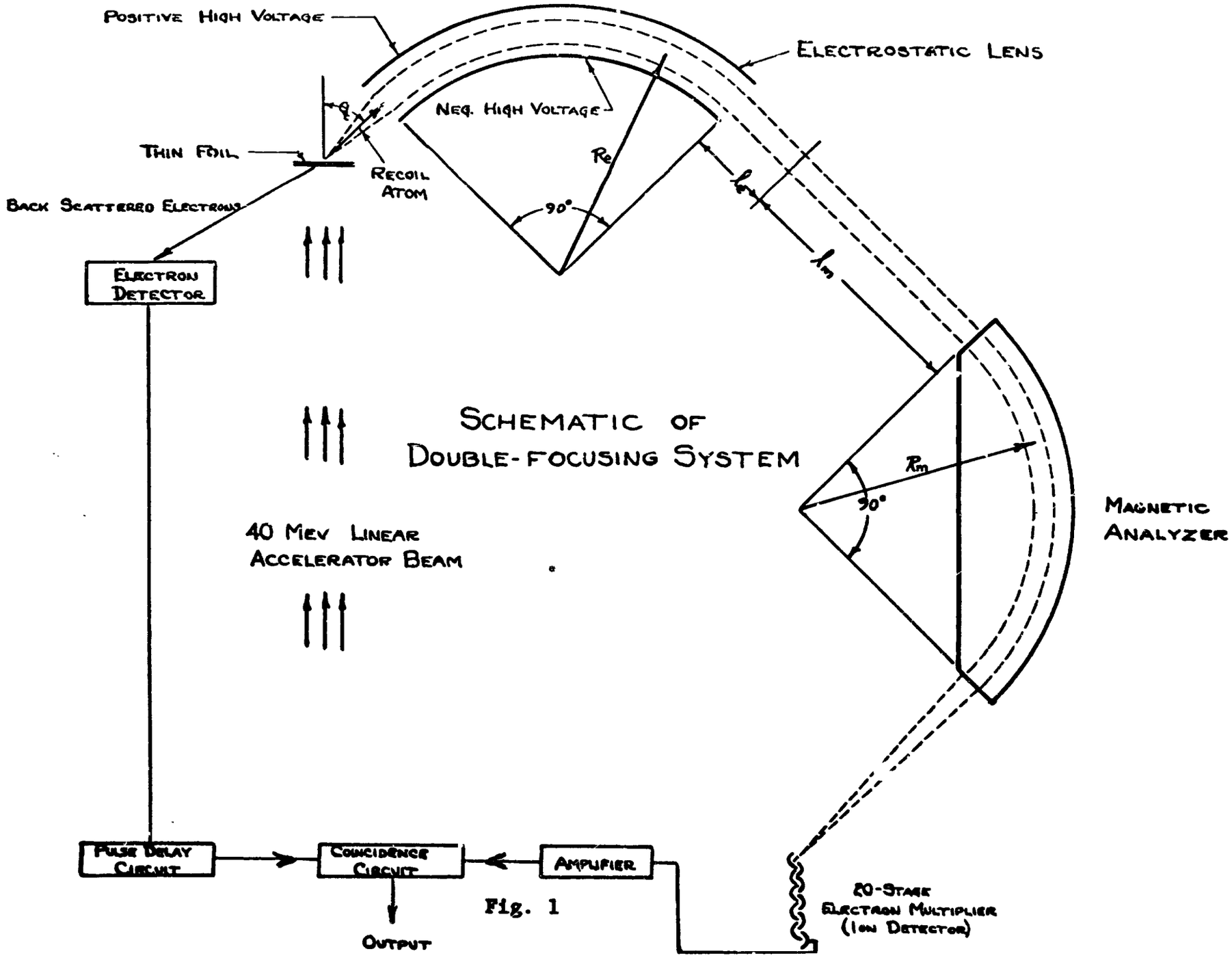
POSITIVE HIGH VOLTAGE
ELECTROSTATIC LENS
NEG. HIGH VOLTAGE
THIN FOIL
RECOIL ATOM
BACK SCATTERED ELECTRONS
ELECTRON DETECTOR
90°
SCHEMATIC OF DOUBLE-FOCUSING SYSTEM
40 MEV LINEAR ACCELERATOR BEAM
MAGNETIC ANALYZER
PULSE DELAY CIRCUIT
COINCIDENCE CIRCUIT
AMPLIFIER
OUTPUT
20-STAGE ELECTRON MULTIPLIER (ION DETECTOR)

Fig. 1

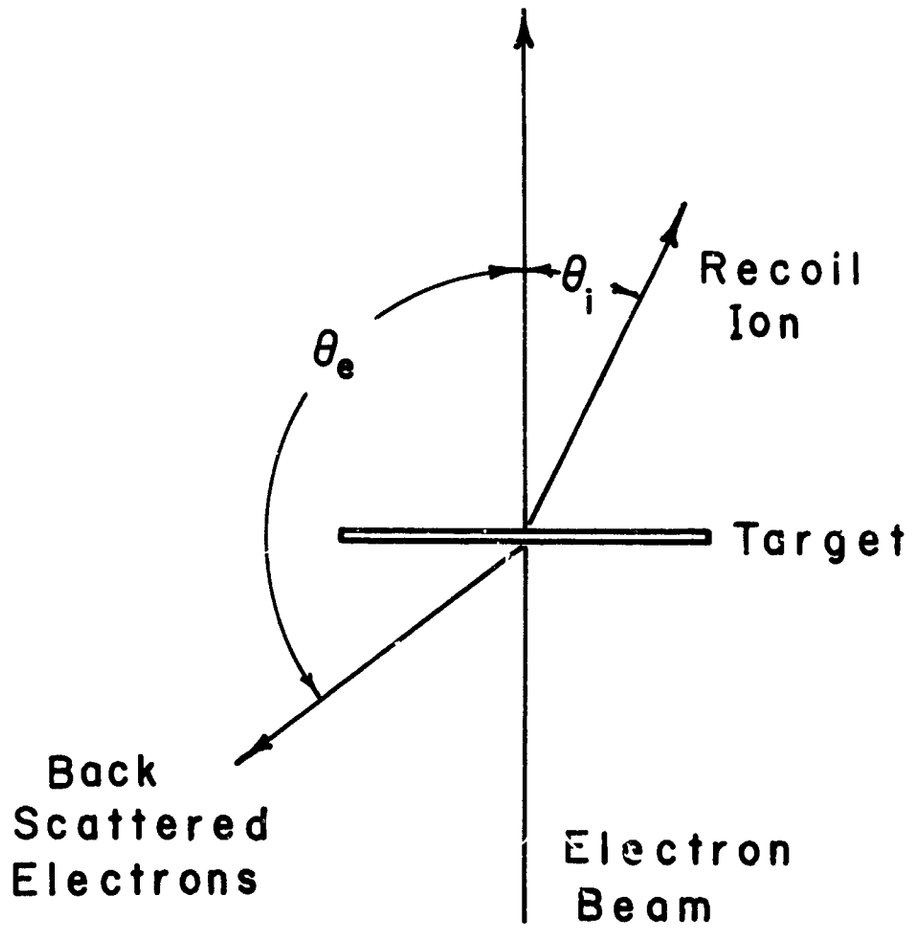

SCATTERING DIAGRAM

Fig. 2

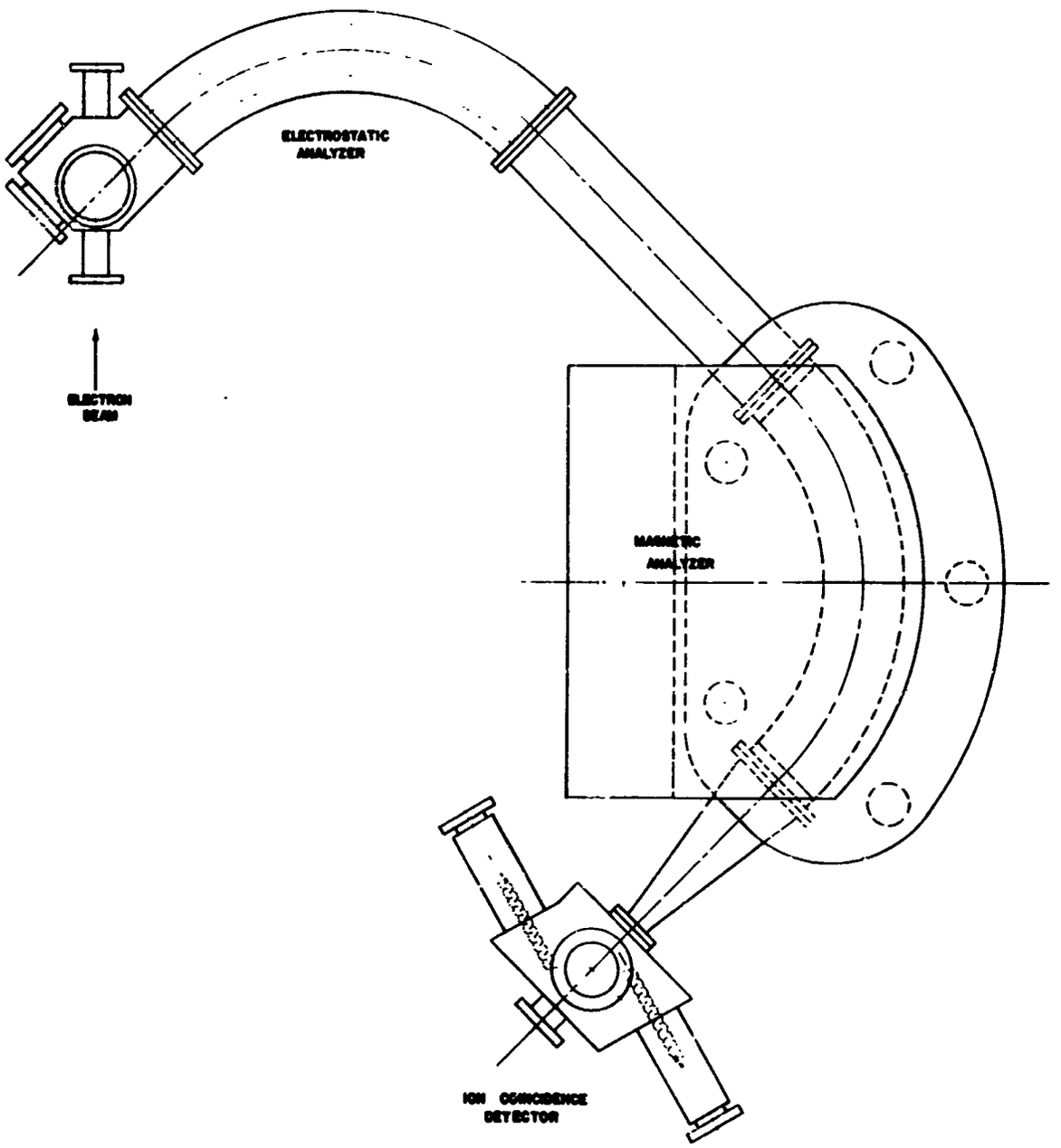
ELECTROSTATIC
ANALYZER
ELECTRON
BEAM
MAGNETIC
ANALYZER
ION COINCIDENCE
DETECTOR

Fig. 3

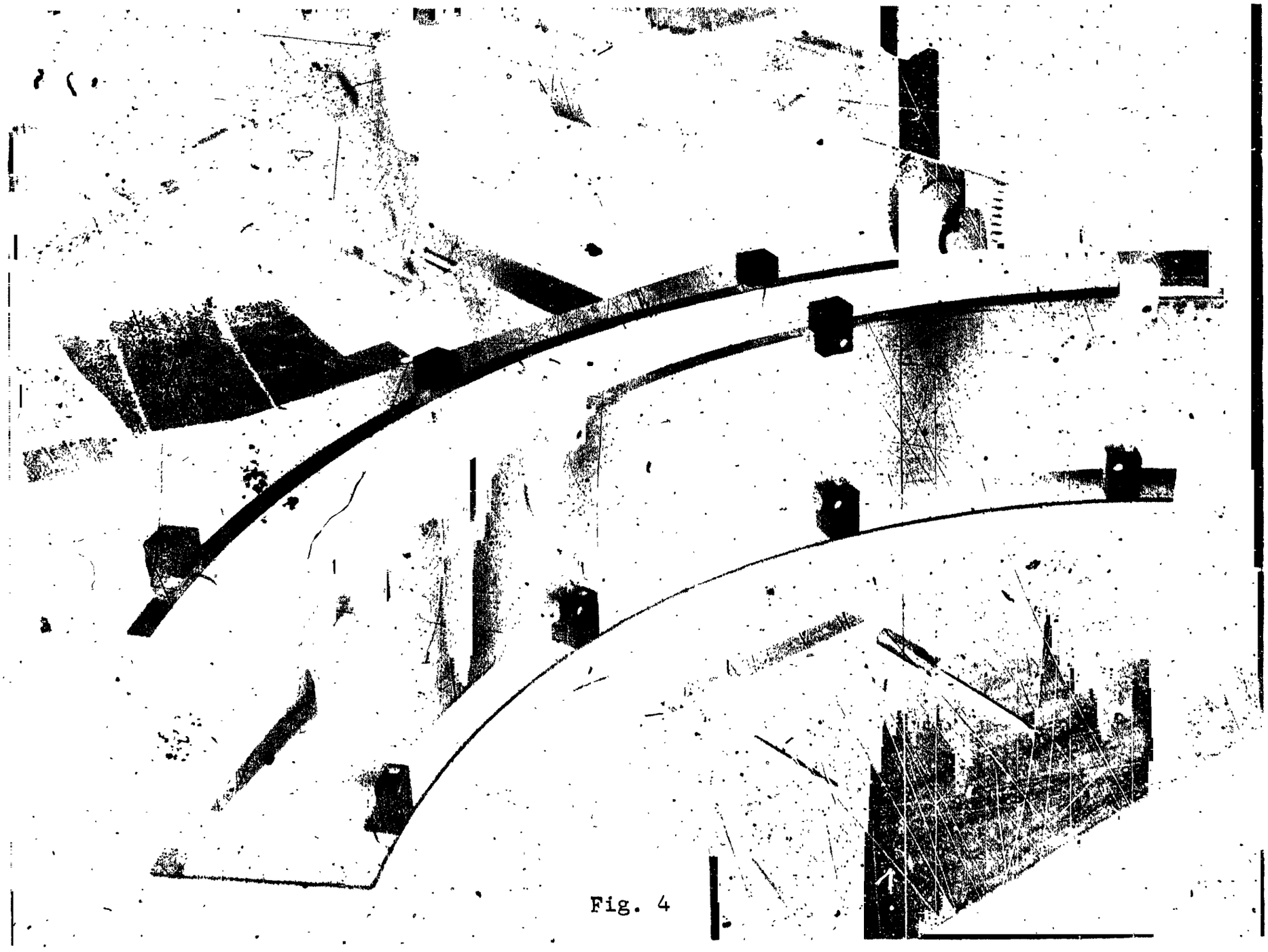

Fig. 4

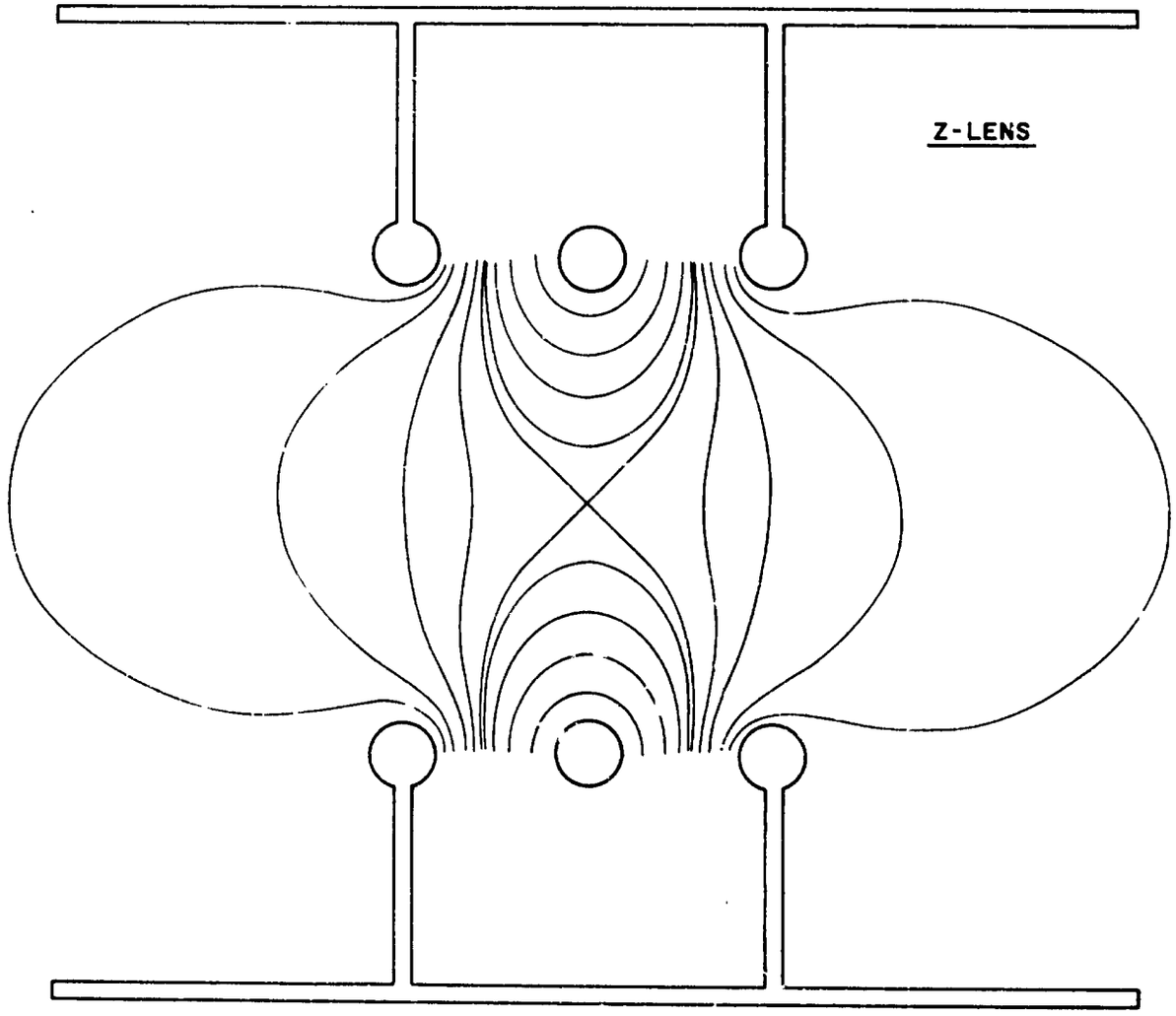

Fig. 5

Fig. 6

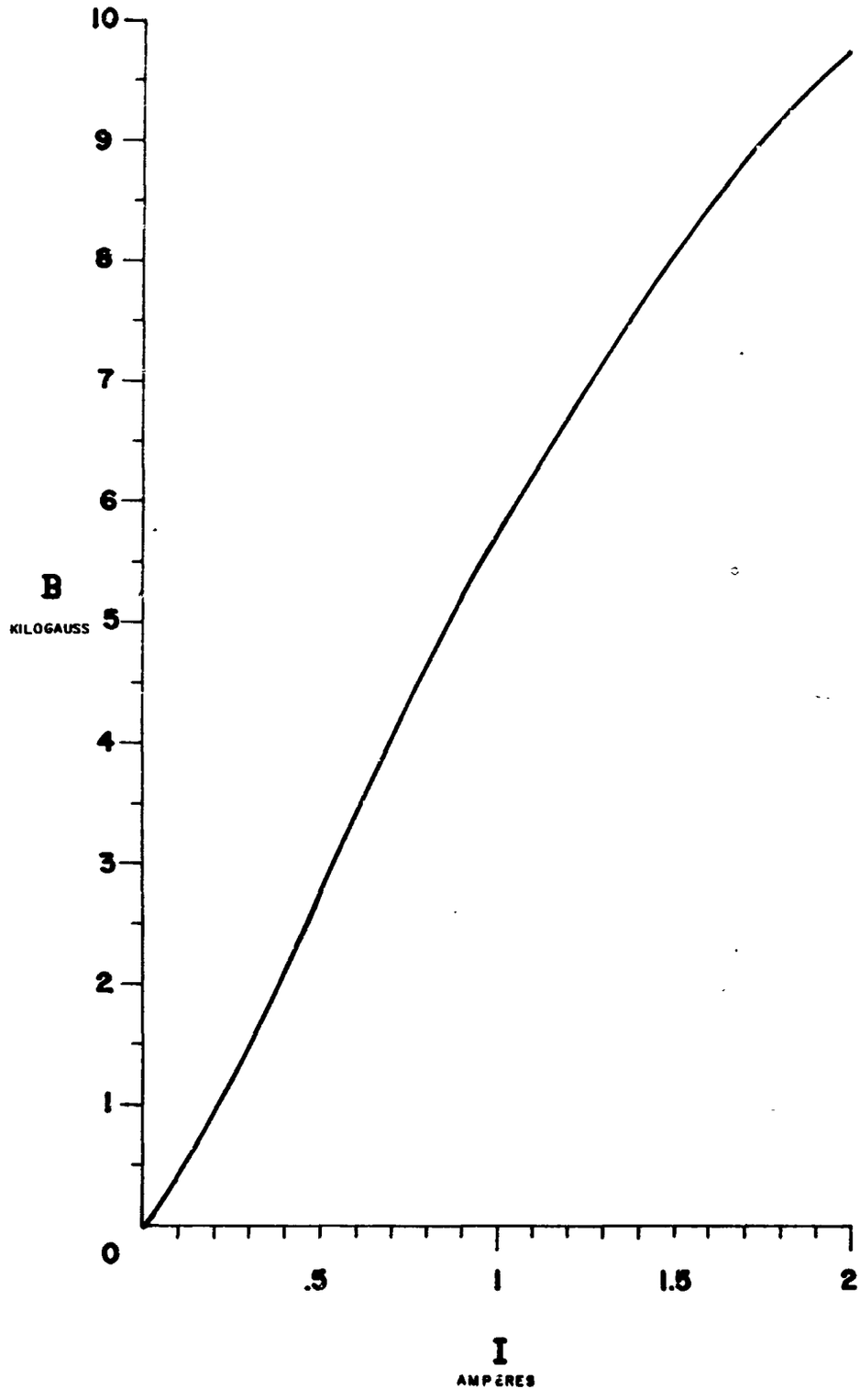

Fig. 7a

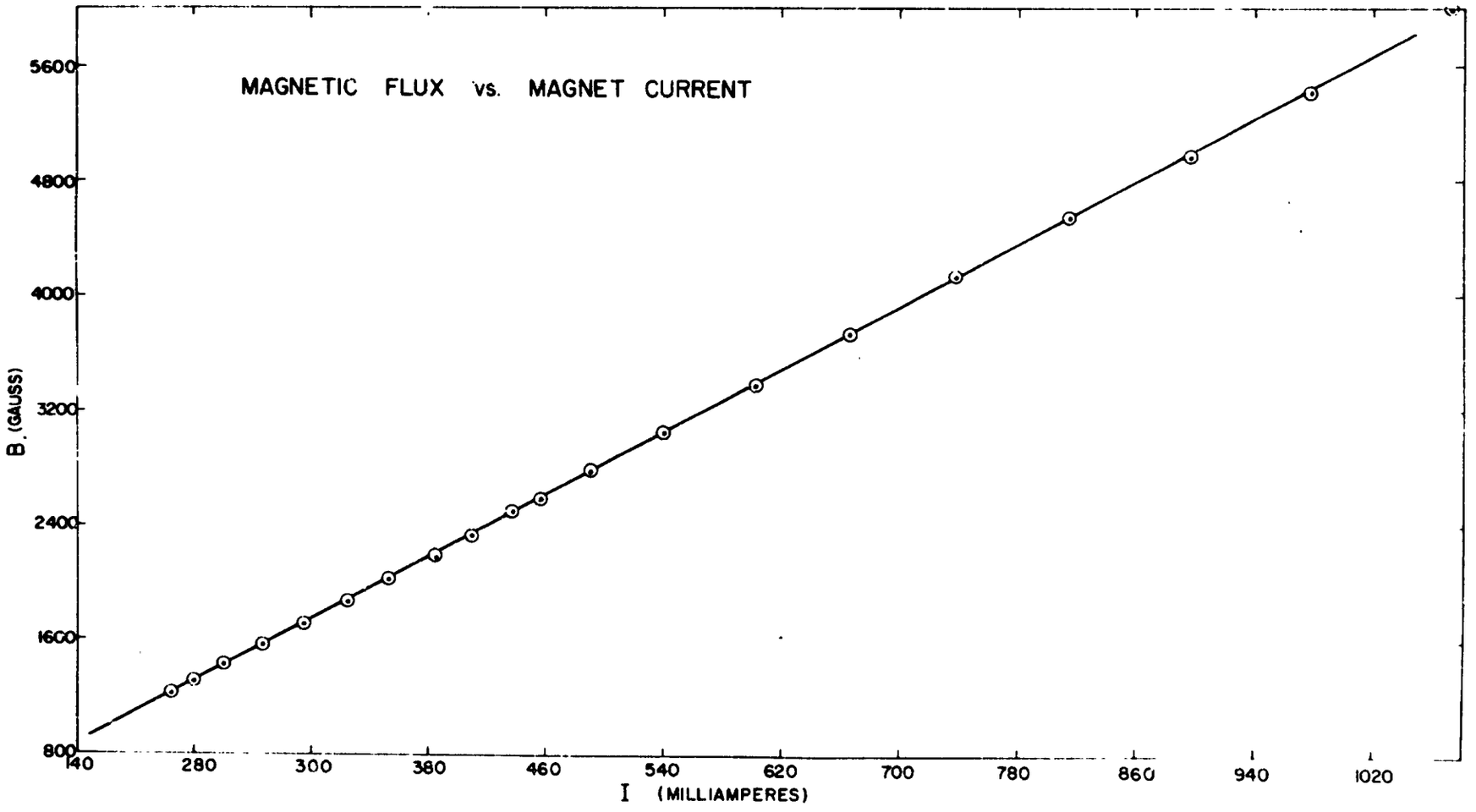
MAGNETIC FLUX vs. MAGNET CURRENT
B (GAUSS)
5600
4800
4000
3200
2400
1600
800
140
280
300
380
460
540
620
700
780
860
940
1020
I (MILLIAMPERES)

Fig. 7b

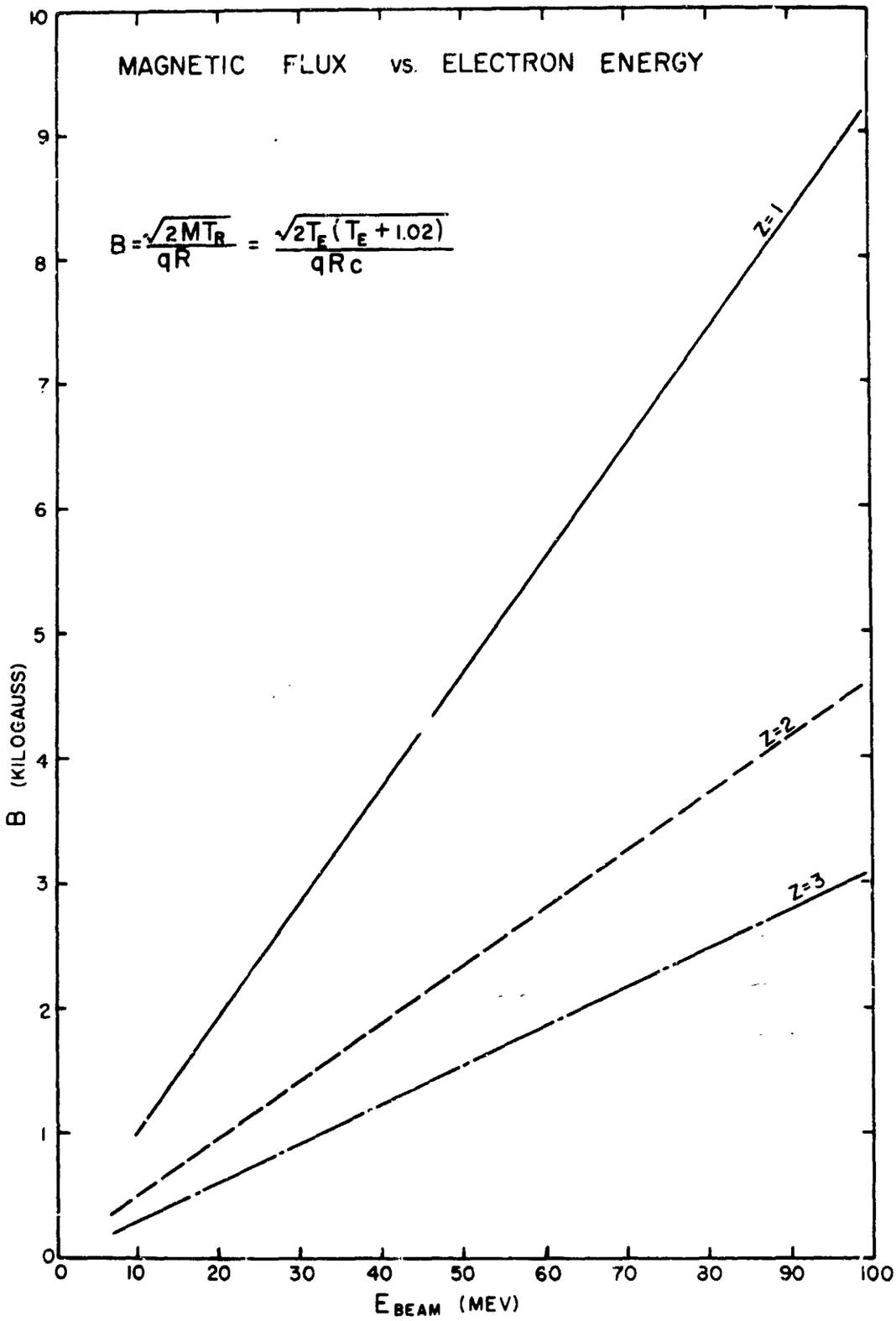
MAGNETIC FLUX vs. ELECTRON ENERGY
$B = \frac{\sqrt{2MT_R}}{qR} = \frac{\sqrt{2T_E(T_E + 1.02)}}{qRc}$
Z=1
Z=2
Z=3
B (KILOGAUSS)
E_{BEAM} (MEV)
0
1
2
3
4
5
6
7
8
9
10
0
10
20
30
40
50
60
70
80
90
100

Fig. 8

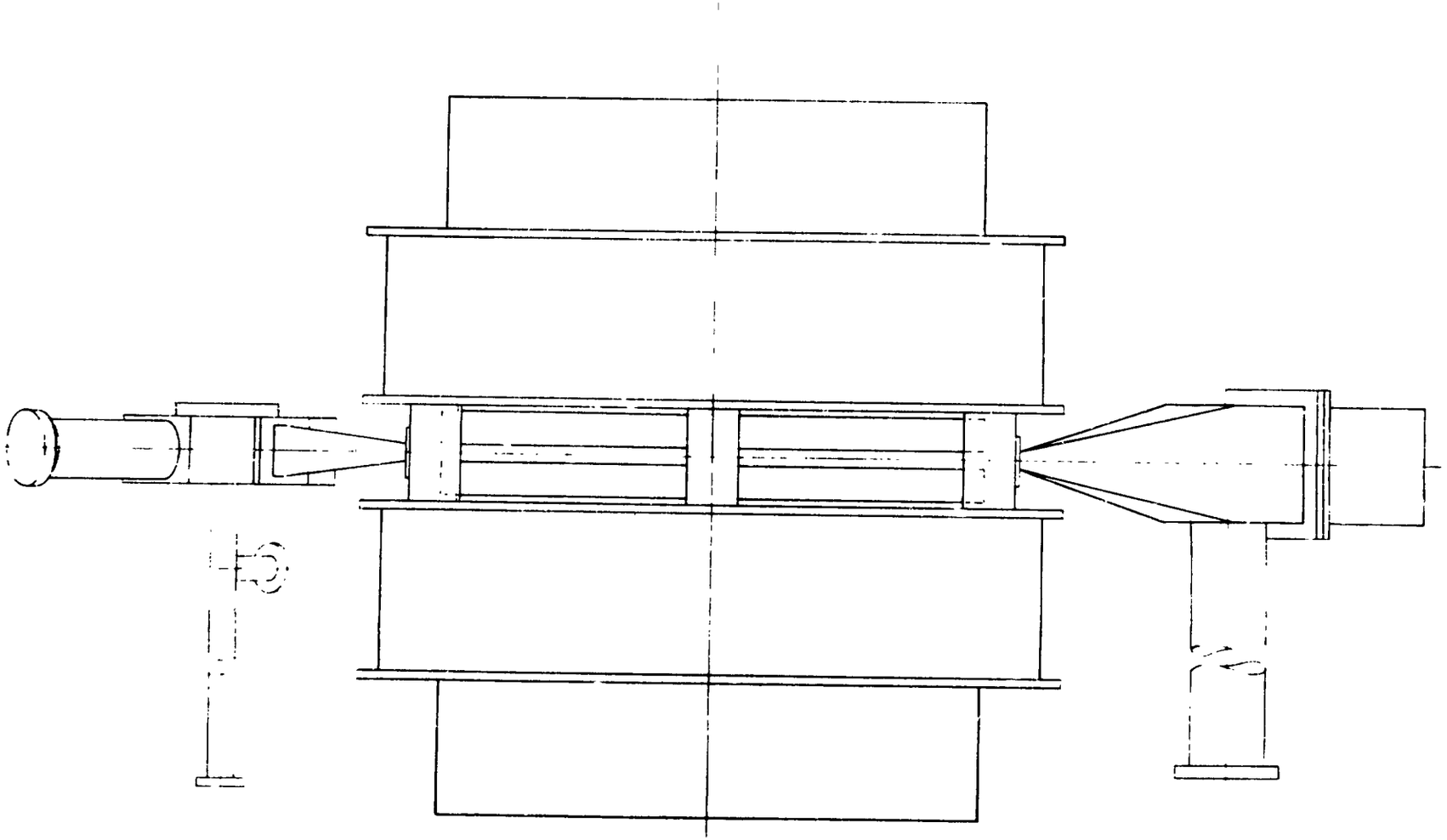

Fig. 9a

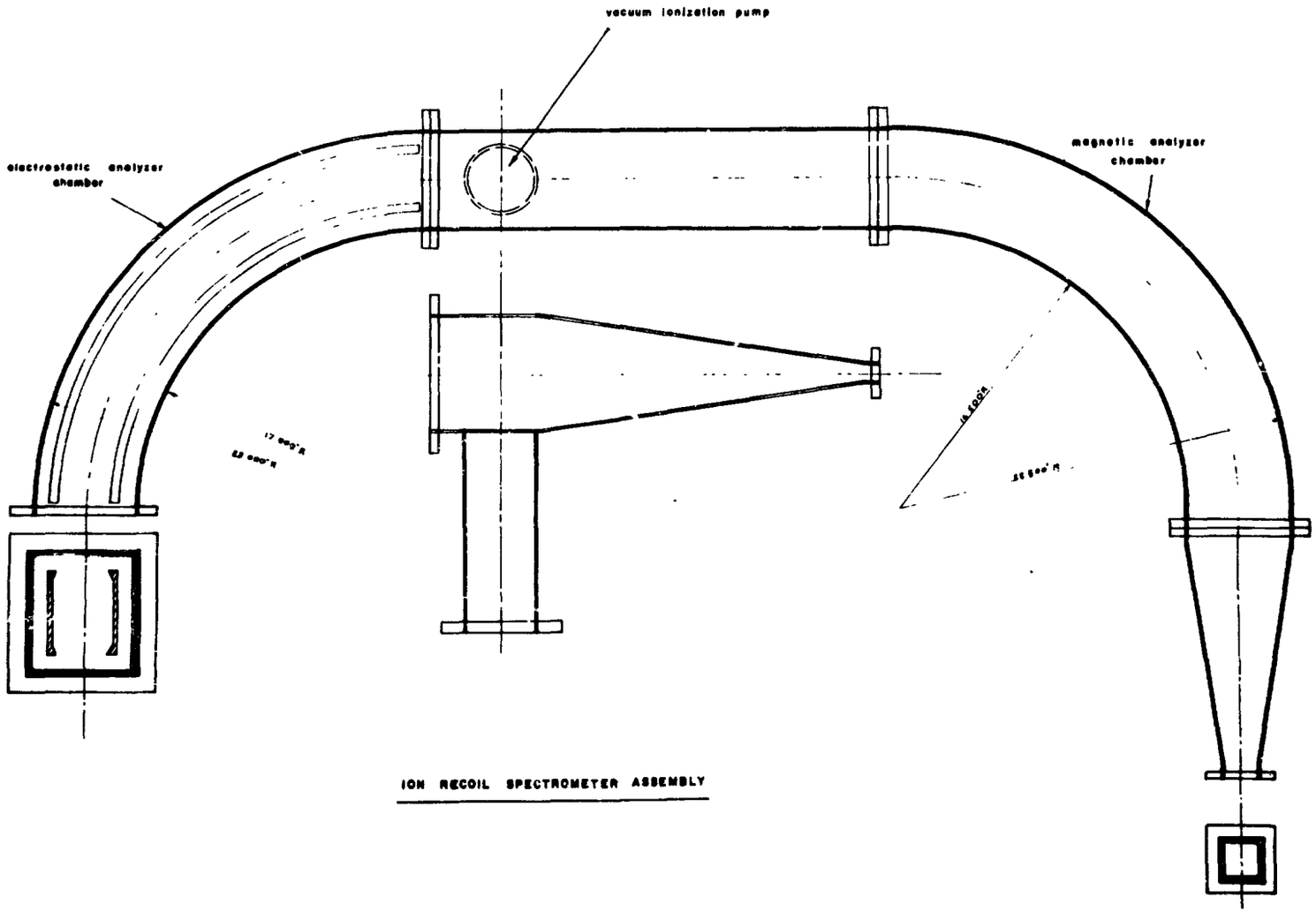

ION RECOIL SPECTROMETER ASSEMBLY

Fig. 9b

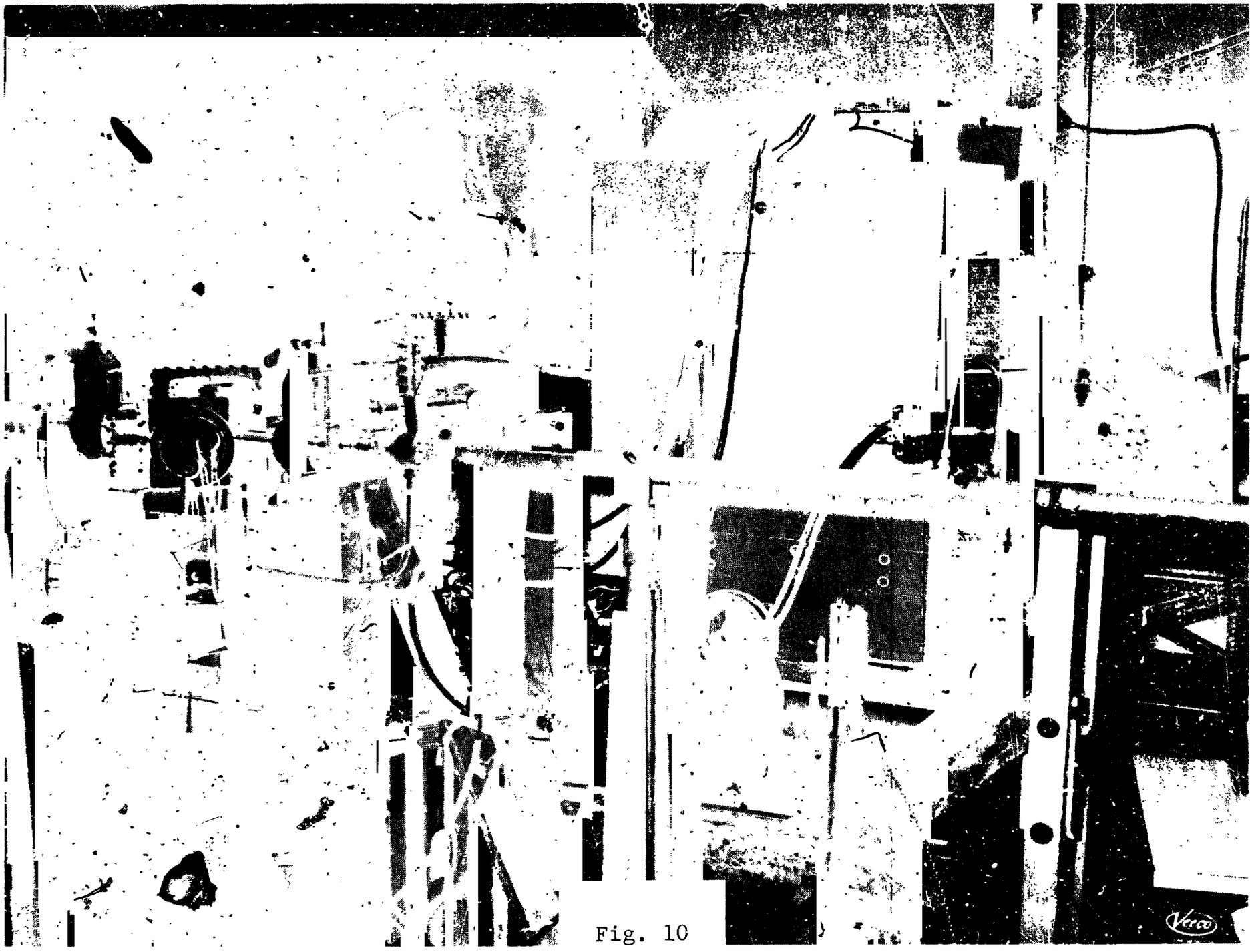

Fig. 10

Fig. 11

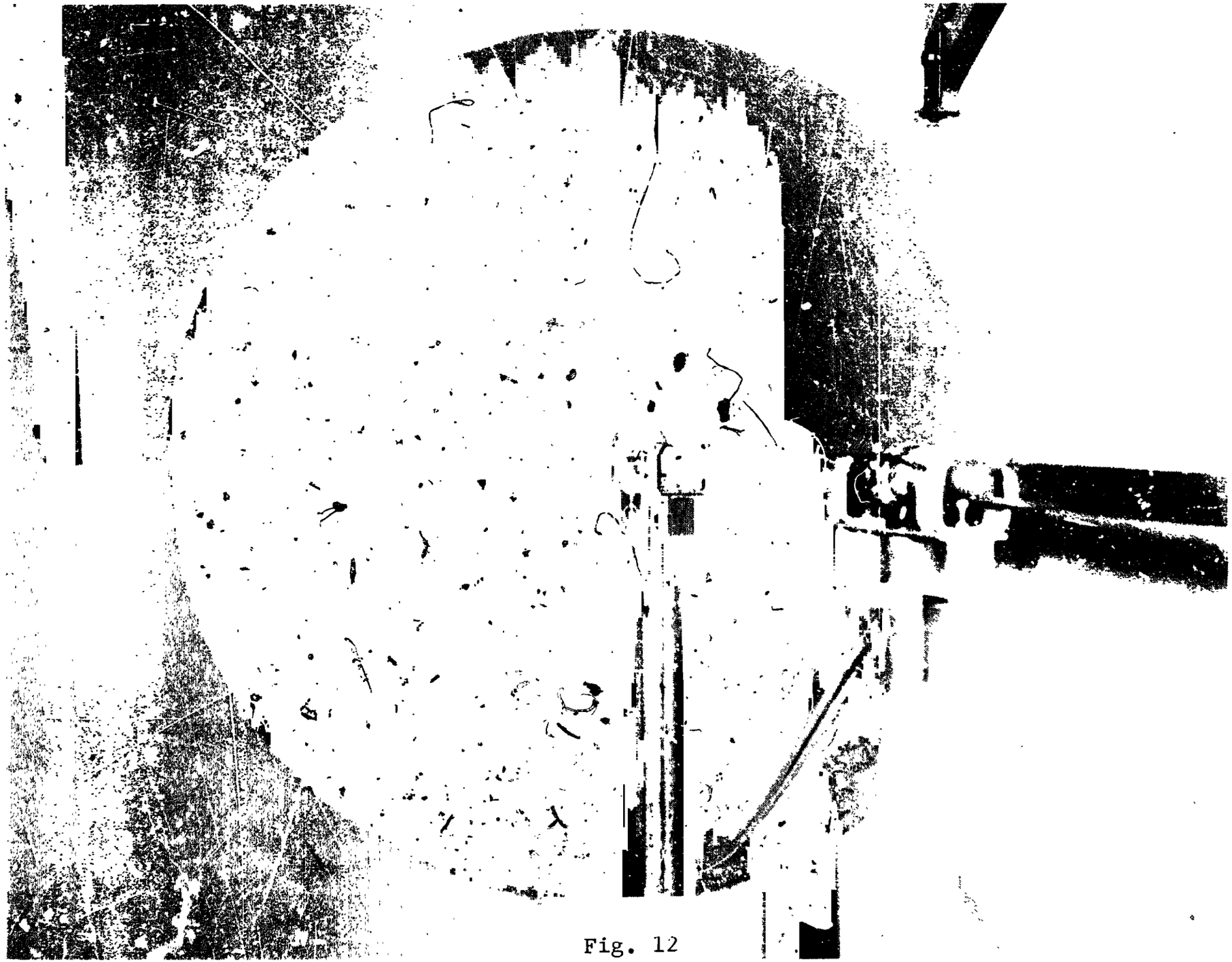

Fig. 12

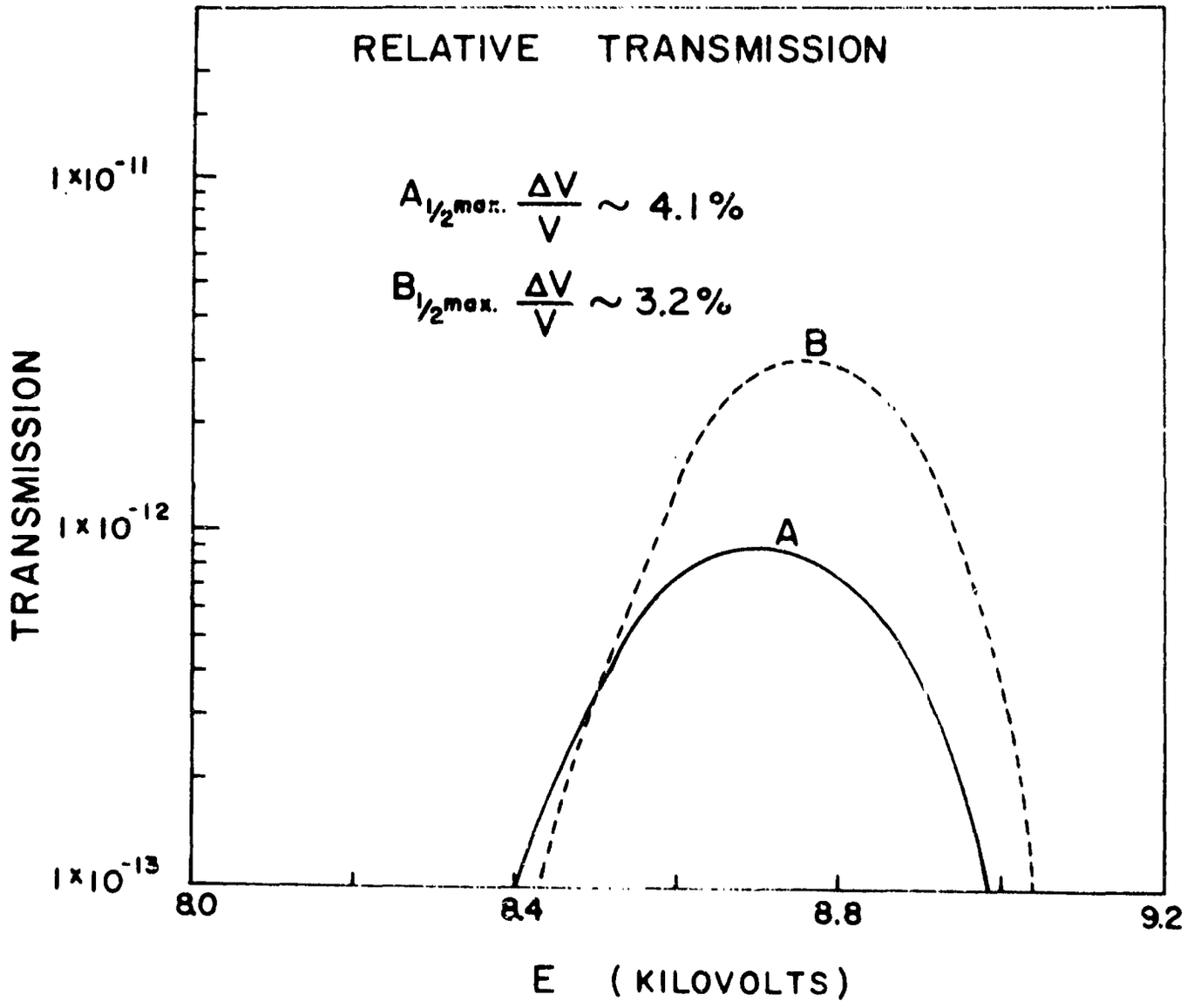
RELATIVE TRANSMISSION
$A_{1/2 max.} \frac{\Delta V}{V} \sim 4.1\%$
$B_{1/2 max.} \frac{\Delta V}{V} \sim 3.2\%$
B
A
TRANSMISSION
1×10^{-11}
1×10^{-12}
1×10^{-13}
8.0
8.4
8.8
9.2
E (KILOVOLTS)

Fig. 13

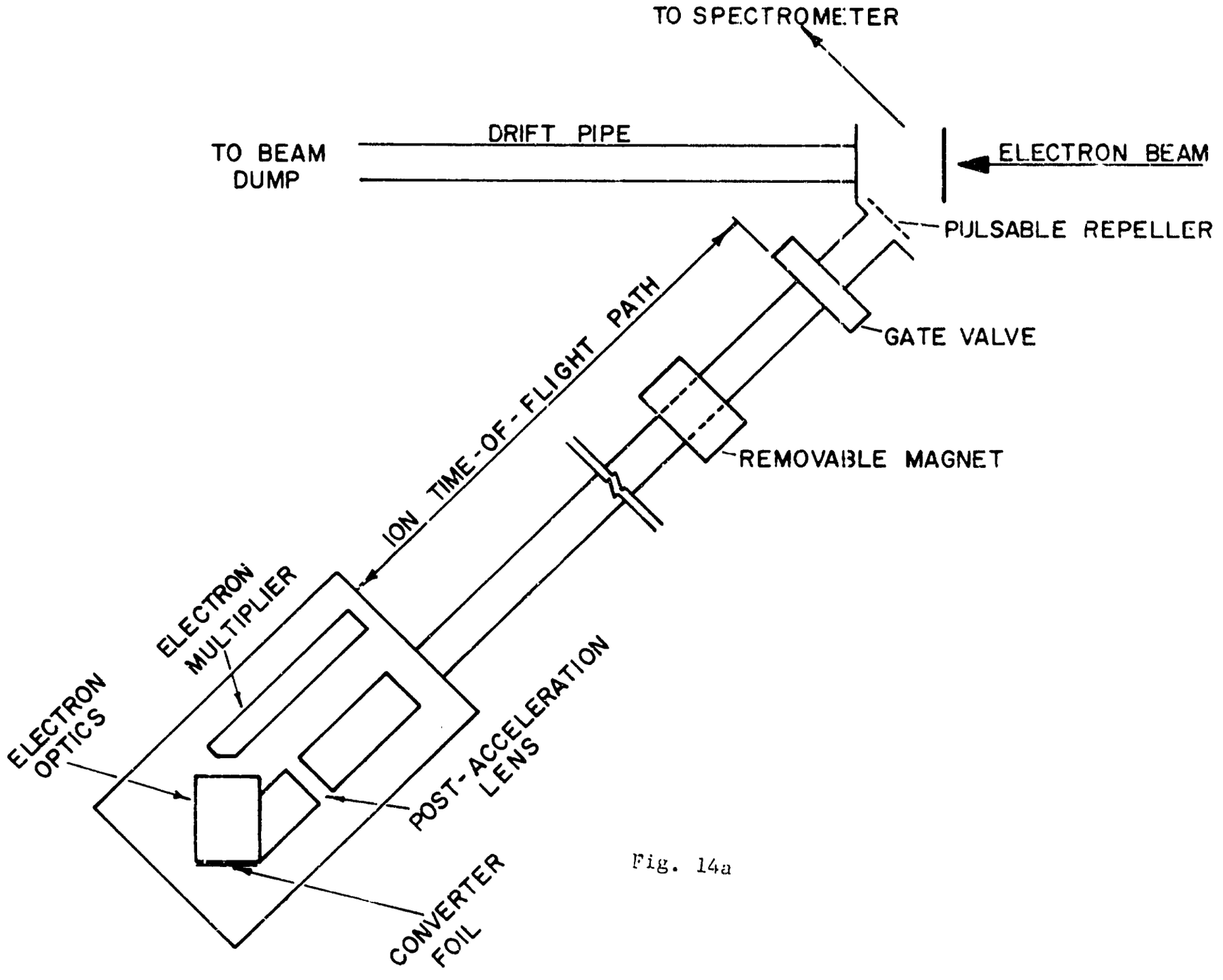
TO SPECTROMETER
DRIFT PIPE
TO BEAM DUMP
ELECTRON BEAM
PULSABLE REPELLER
GATE VALVE
ION TIME-OF-FLIGHT PATH
REMOVABLE MAGNET
ELECTRON MULTIPLIER
ELECTRON OPTICS
POST-ACCELERATION LENS
CONVERTER FOIL

Fig. 14a

ION RECOIL
TIME-OF-FLIGHT LEG

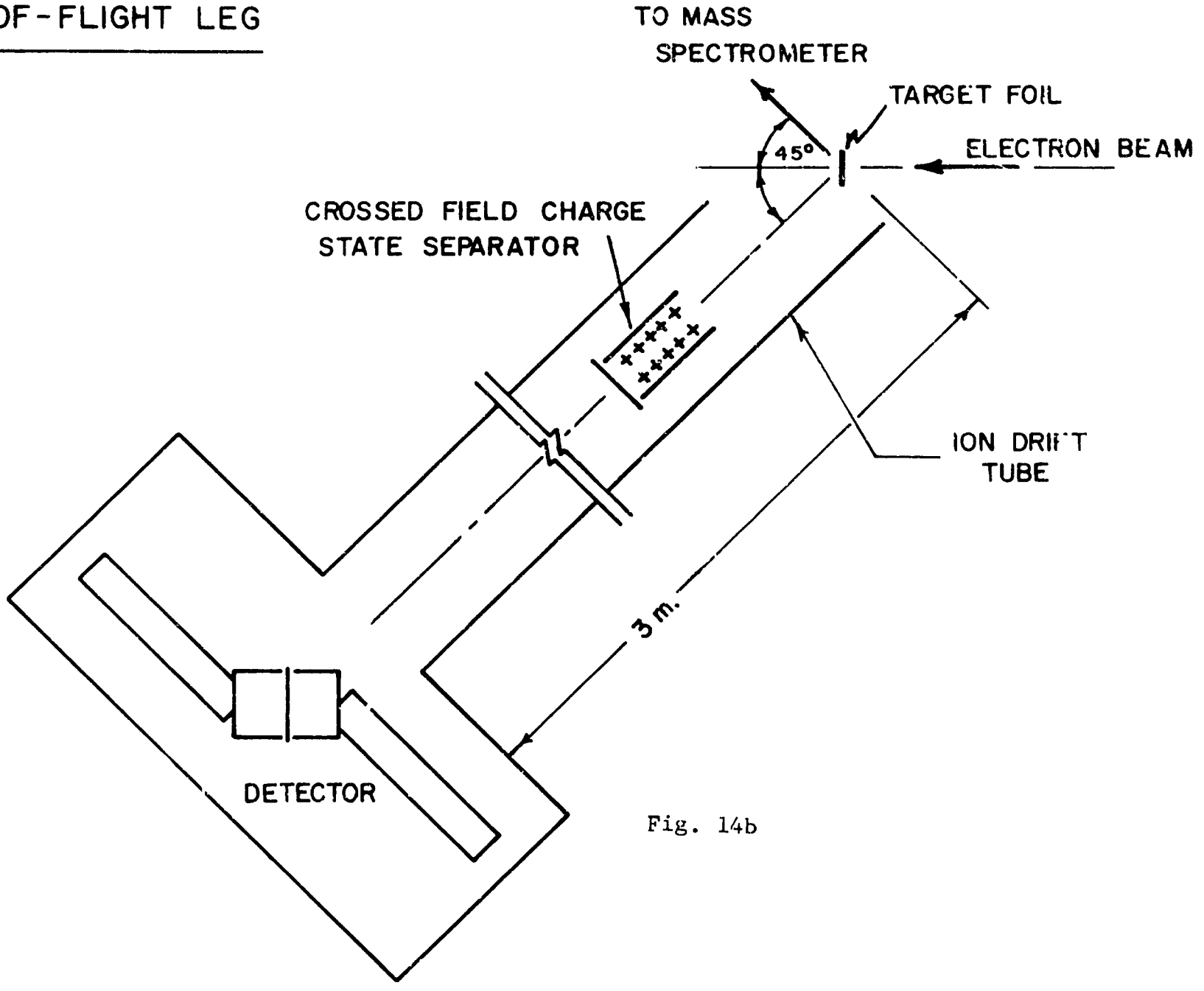

Fig. 14b

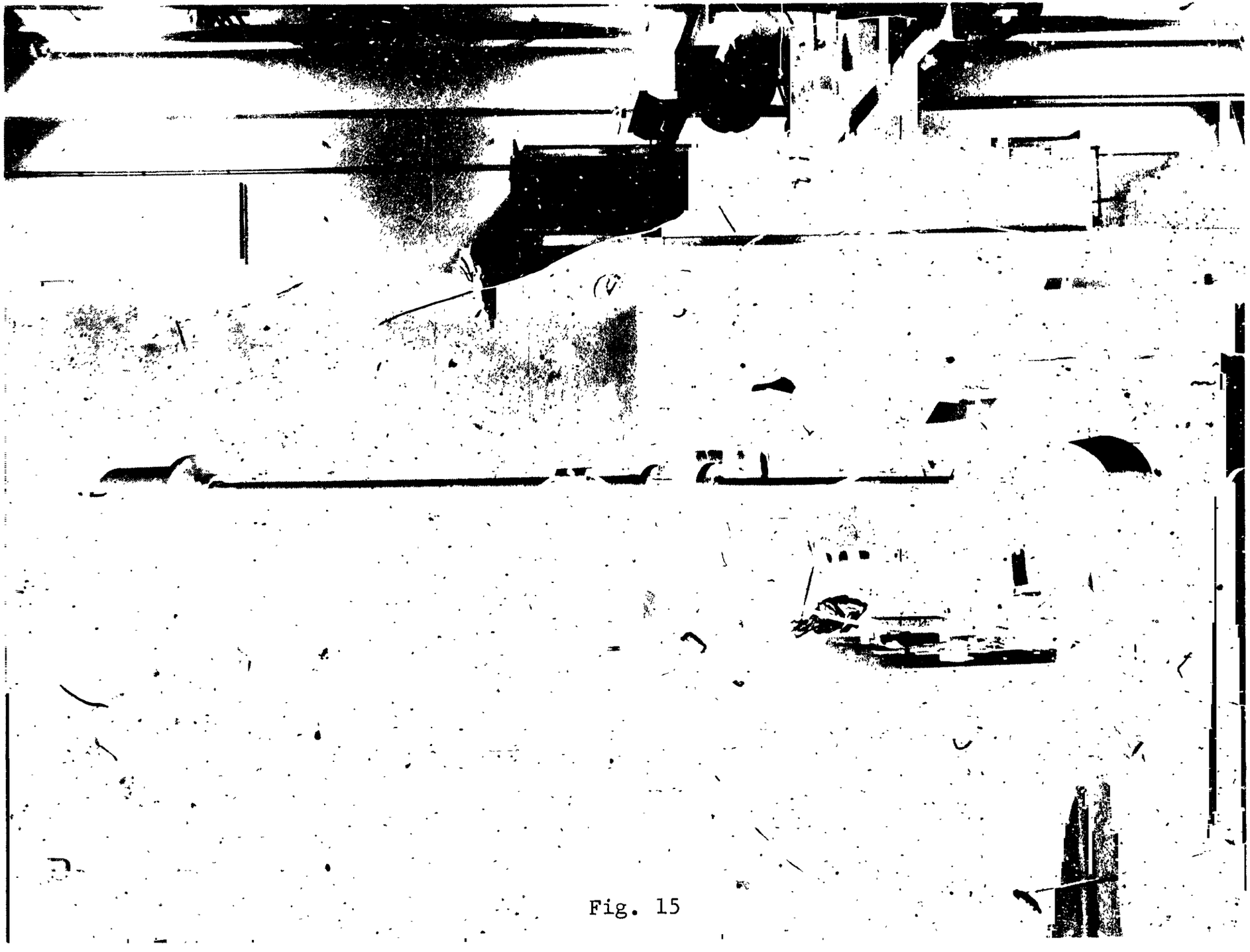

Fig. 15

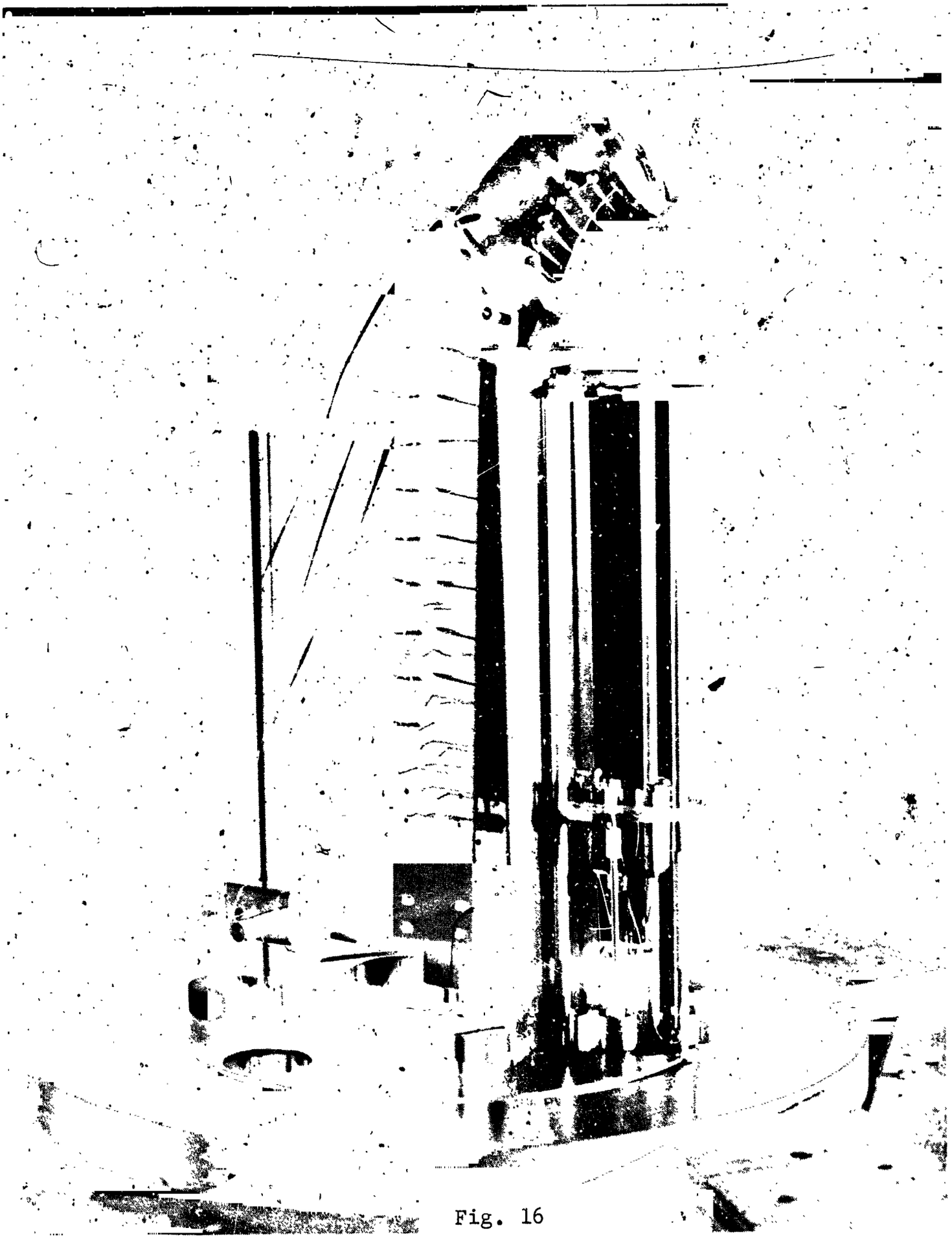

Fig. 16

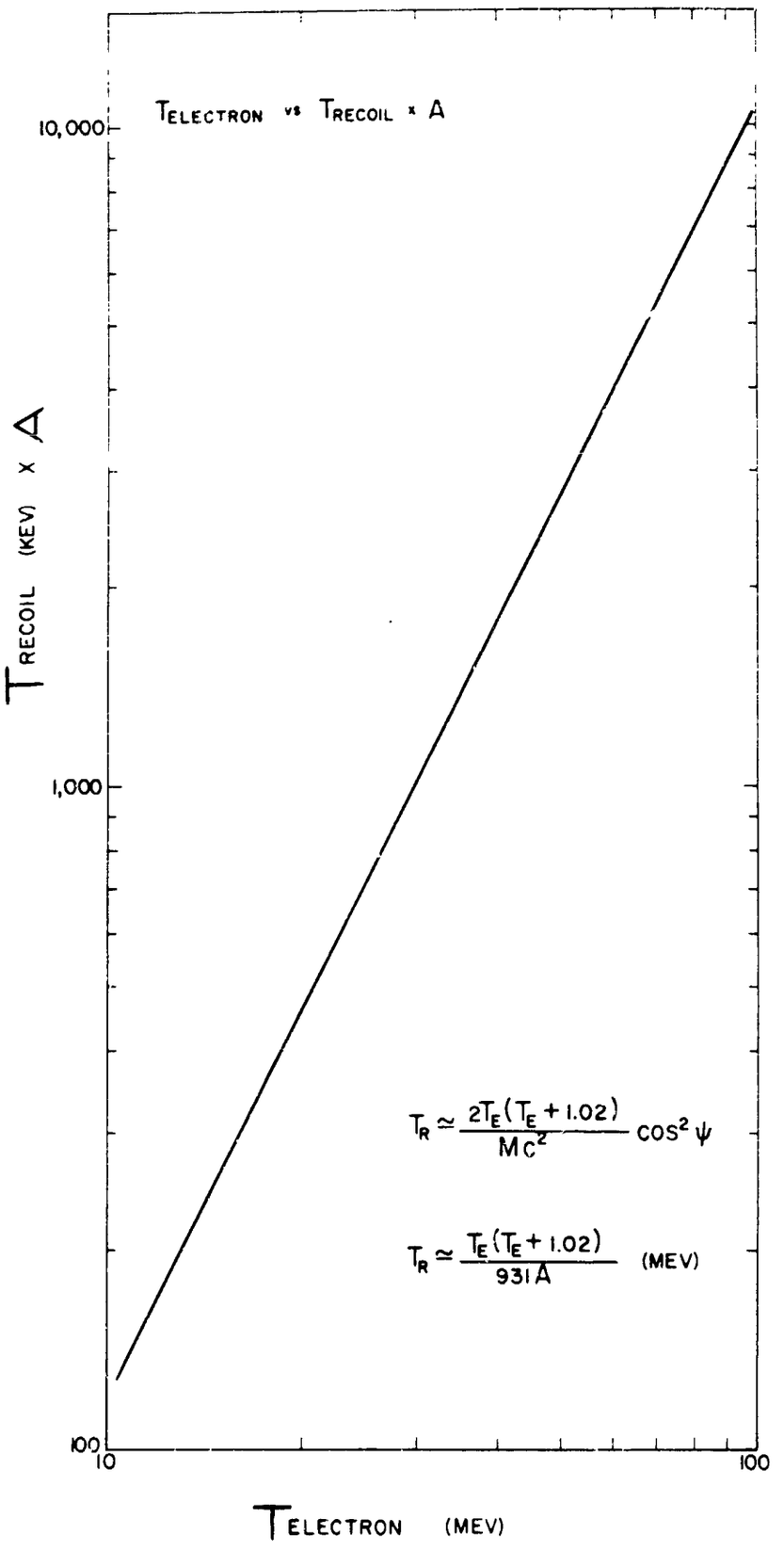
T ELECTRON vs T RECOIL x A
10,000
1,000
100
10
100
T RECOIL (KEV) x A
T ELECTRON (MEV)
$T_R \simeq \frac{2T_E(T_E+1.02)}{Mc^2}\cos^2\psi$
$T_R \simeq \frac{T_E(T_E+1.02)}{931A}$ (MEV)

Fig. 17

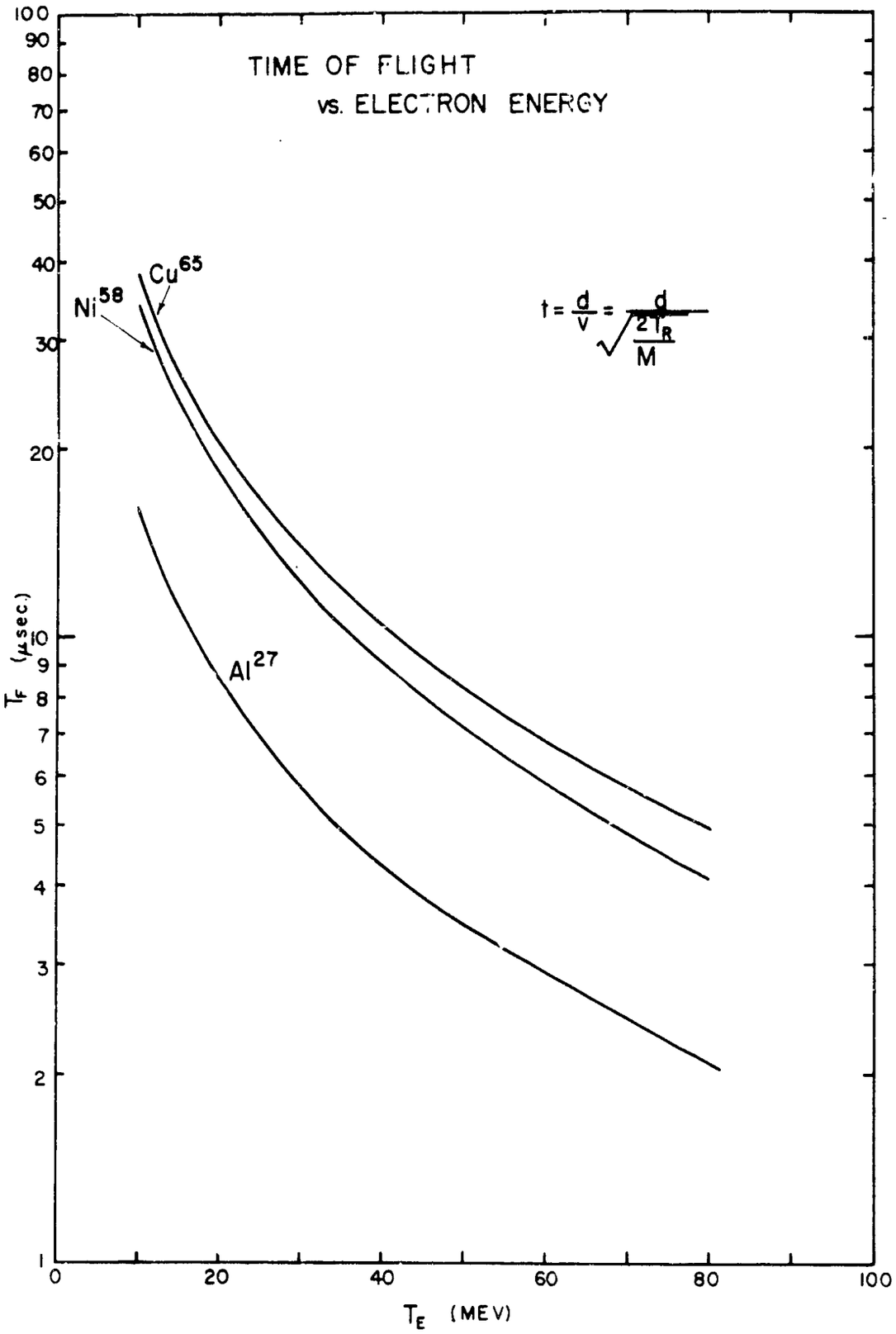
TIME OF FLIGHT
vs. ELECTRON ENERGY
$t = \frac{d}{v} = \frac{d}{\sqrt{\frac{2T_R}{M}}}$
Cu65
Ni58
Al27
T_F (μsec.)
T_E (MEV)
100
90
80
70
60
50
40
30
20
10
9
8
7
6
5
4
3
2
1
0
20
40
60
80
100

Fig. 18

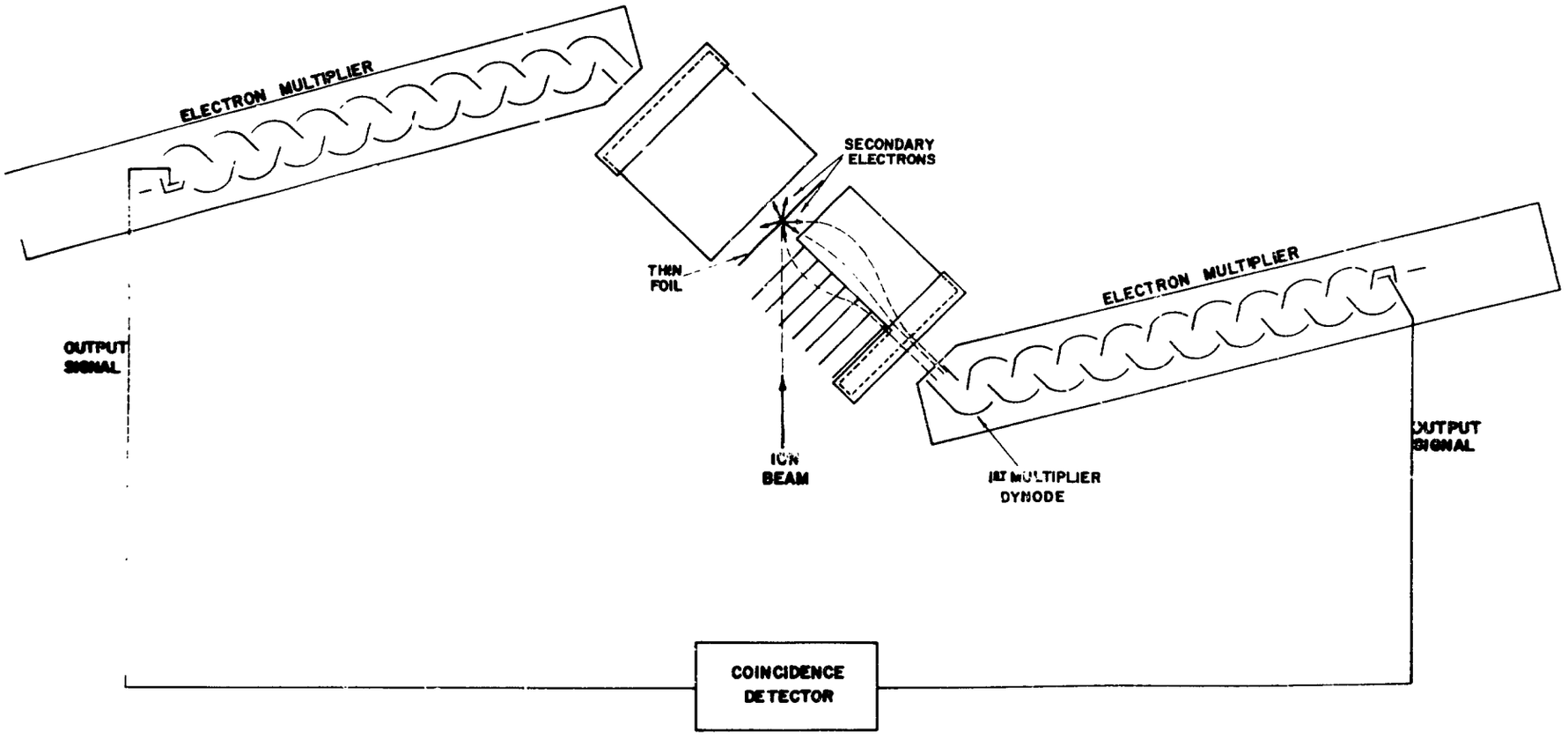
ELECTRON MULTIPLIER
SECONDARY ELECTRONS
THIN FOIL
ELECTRON MULTIPLIER
OUTPUT SIGNAL
ION BEAM
MULTIPLIER DYNODE
OUTPUT SIGNAL
COINCIDENCE DETECTOR

Fig. 19

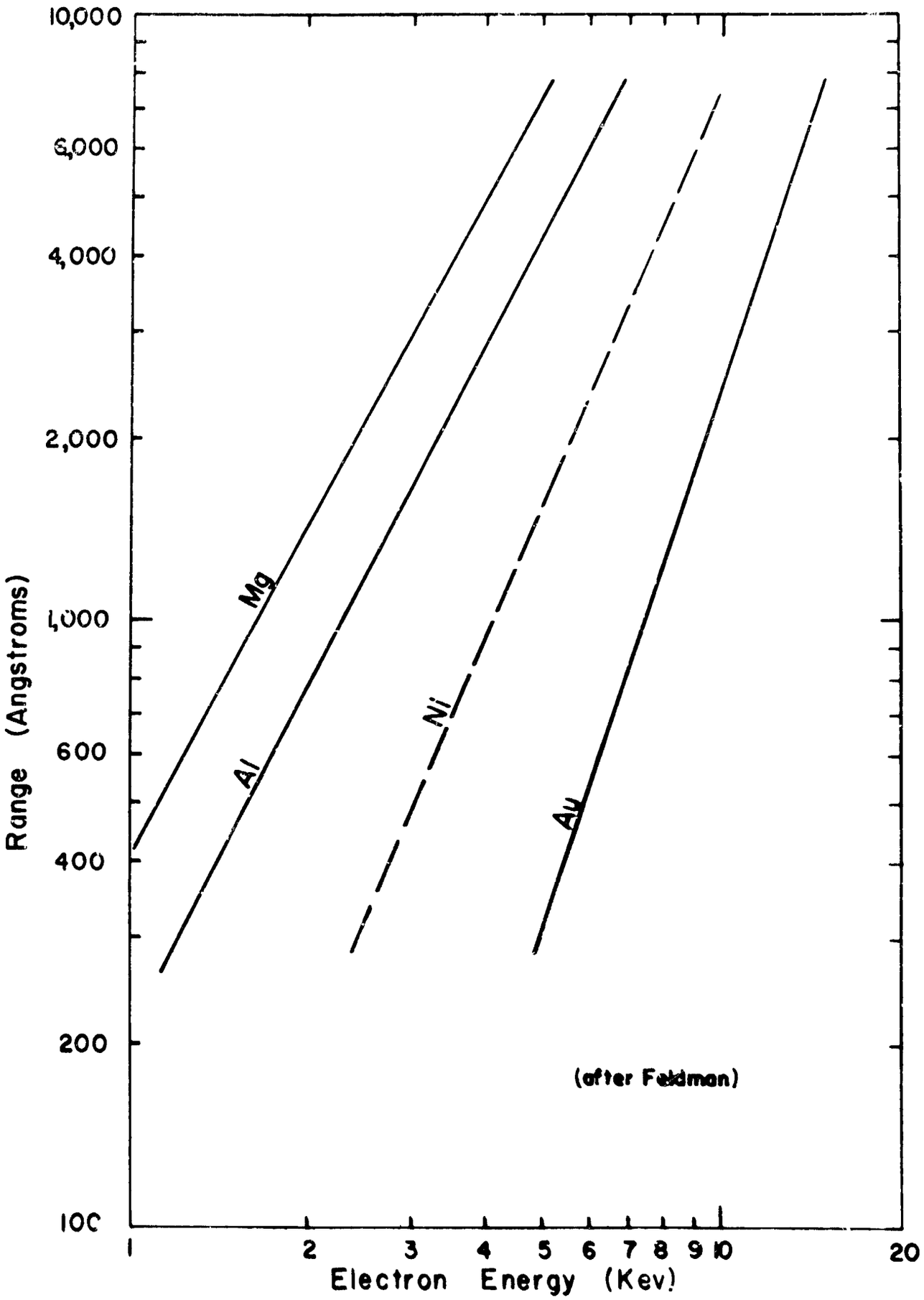
10,000
6,000
4,000
2,000
1,000
600
400
200
100
Range (Angstroms)
Mg
Al
Ni
Au
(after Feldman)
1
2
3
4
5
6
7
8
9
10
20
Electron Energy (Kev)

Fig. 20

APPROXIMATE RANGE OF POSITIVE IONS IN SILICON (after FERBER)

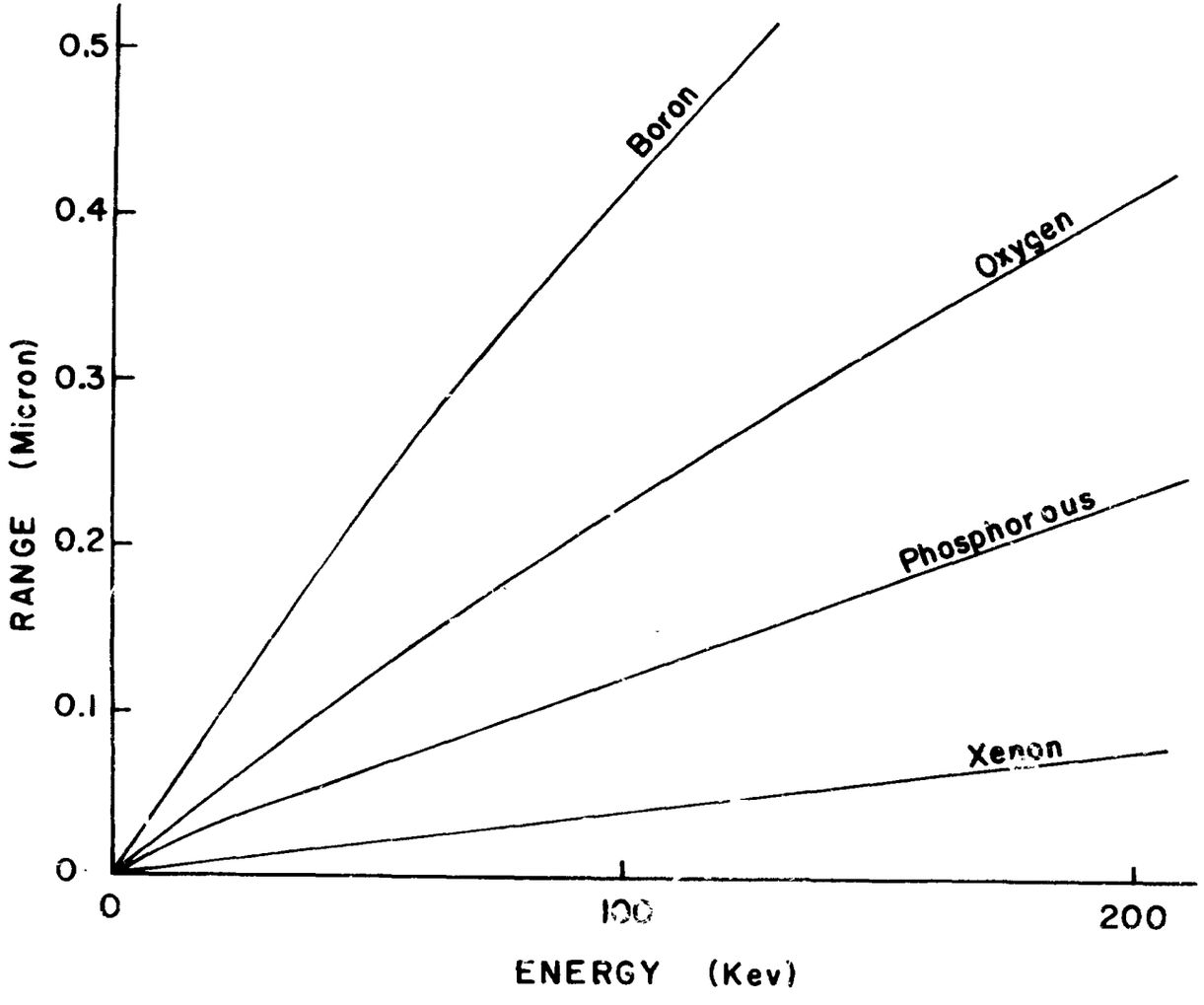

Fig. 21

Median Range of Ions* ($\mu g/cm^2$)

	Energy (Kev)				
	2	5	10	30	60
Na - 24	1.1	3.0	6.2	15	29
A - 41	1	—	—	12	19
K - 42	0.6	1.9	4.0	9.0	13

*(Davies, et al)

Fig. 22

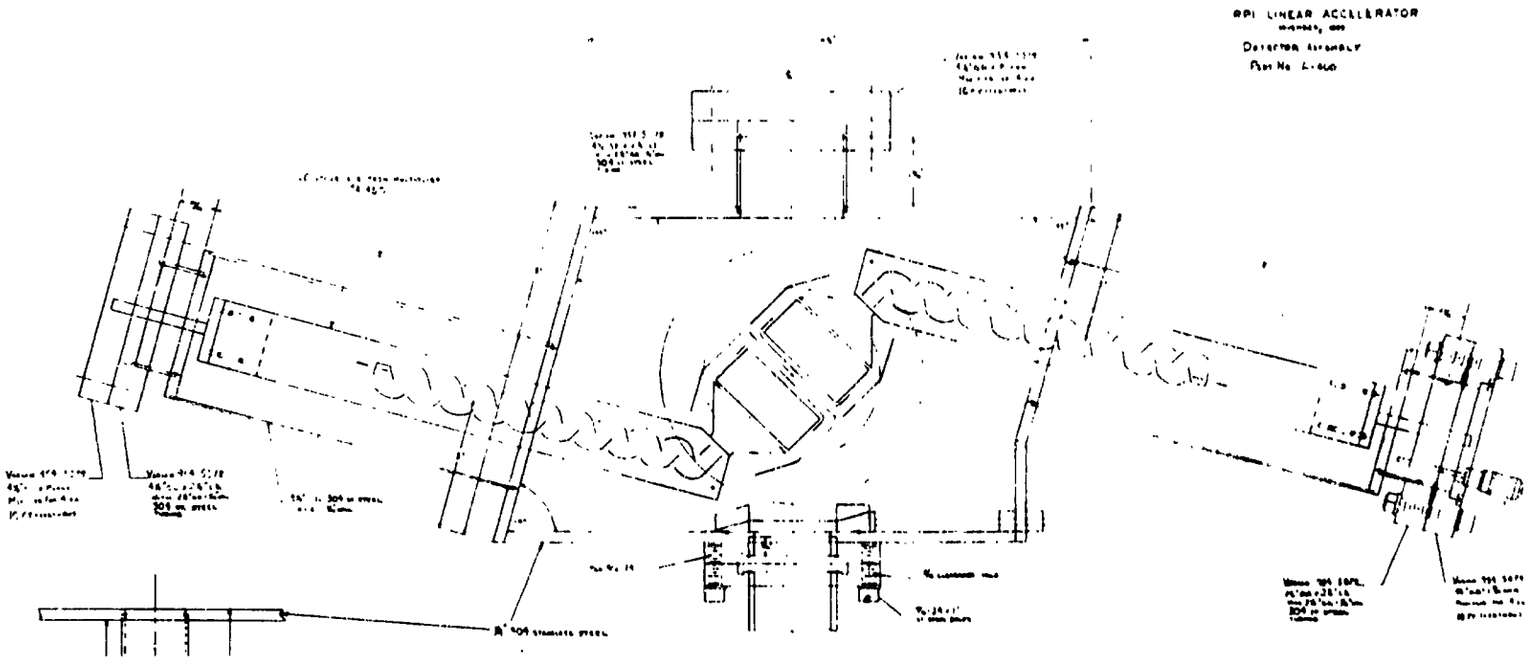

Fig. 23

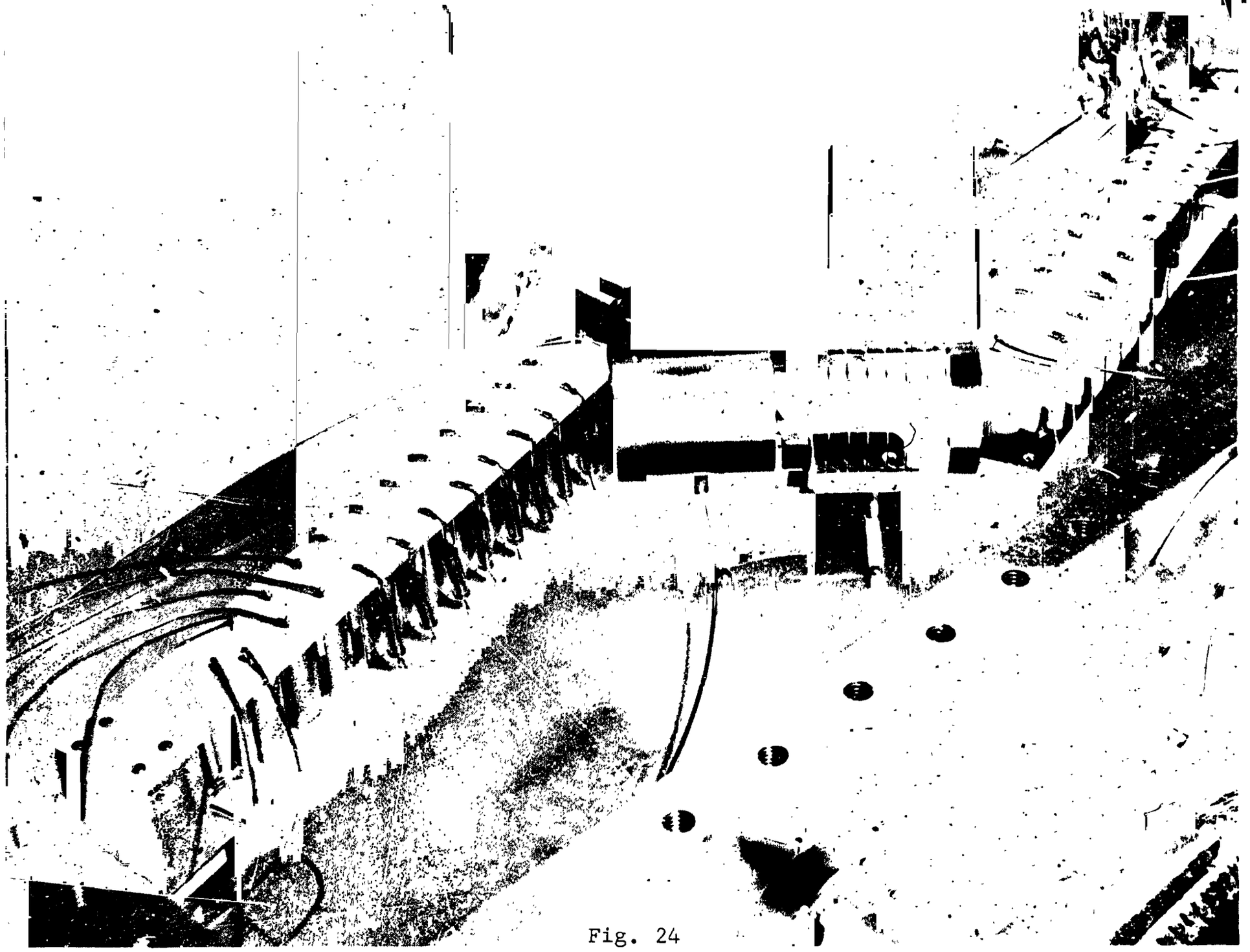

Fig. 24

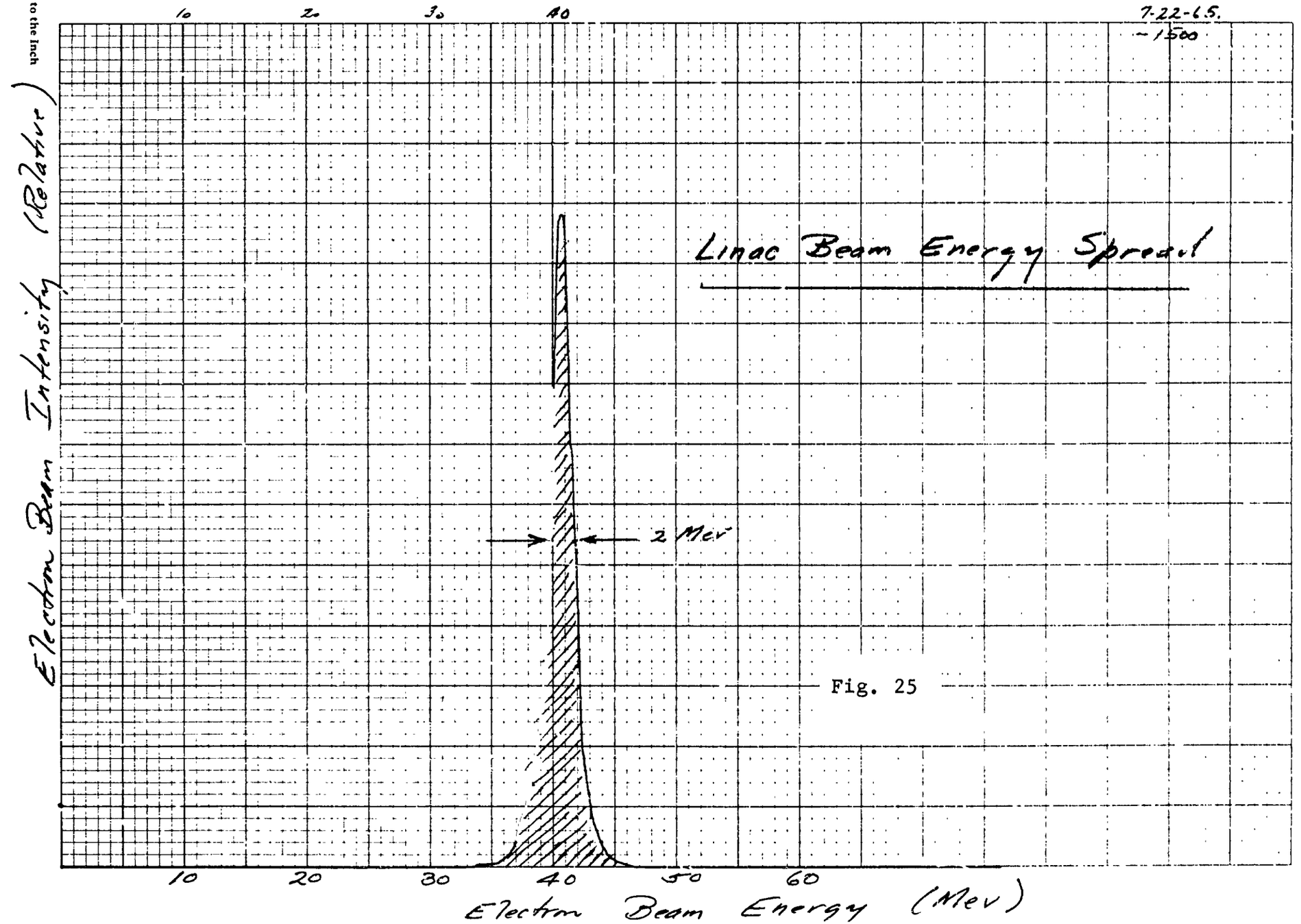
10 Squares to the inch
10
20
30
40
7-22-65.
~1500
Linac Beam Energy Spread
2 Mev
Electron Beam Intensity (Relative)
10
20
30
40
50
60
Electron Beam Energy (Mev)

Fig. 25

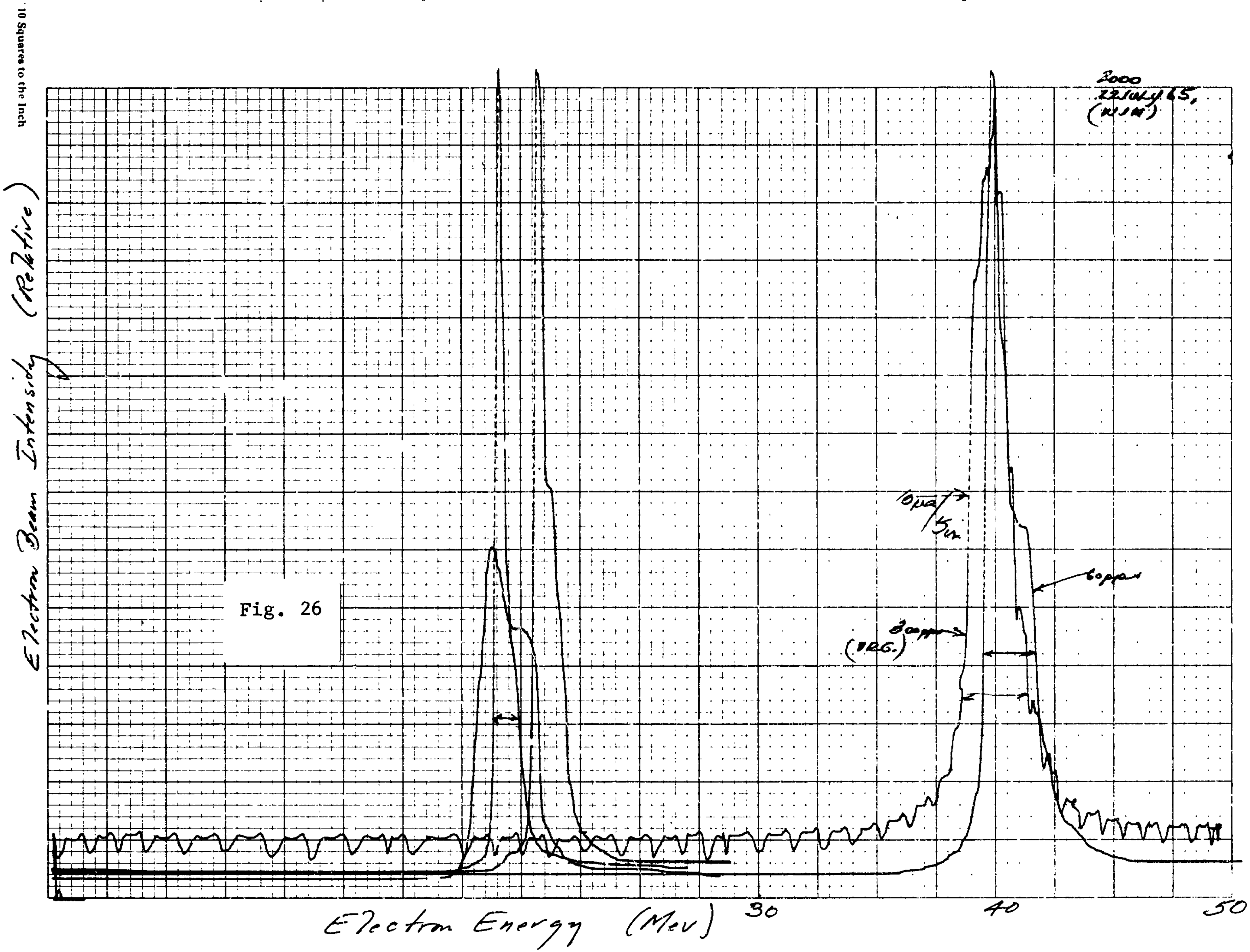

2000
22 July 65,
(WJM)
10μa/½in
6copper
8copper
(VRG.)
30
40
50
Electron Energy (Mev)
Electron Beam Intensity (Relative)
10 Squares to the Inch

Fig. 26

COUNTS
10 μSec - 10³ MACHINE BURSTS
10⁴
10³
10²
0
50
100
150
200
250
ION TIME OF FLIGHT (μSEC.)
RECOIL ENERGY
— 4.1 KEV.
— 1.2 KEV.
— 180 EV.
— 120 EV.
ELASTIC RECOIL: 75 KEV.; 4.7 μSEC.
ALUMINUM
• 0.0003" FOIL
○ 0.0006" FOIL
14 MEV
60 ma
0.25 μs
ELECTRON BEAM BURST

Fig. 27

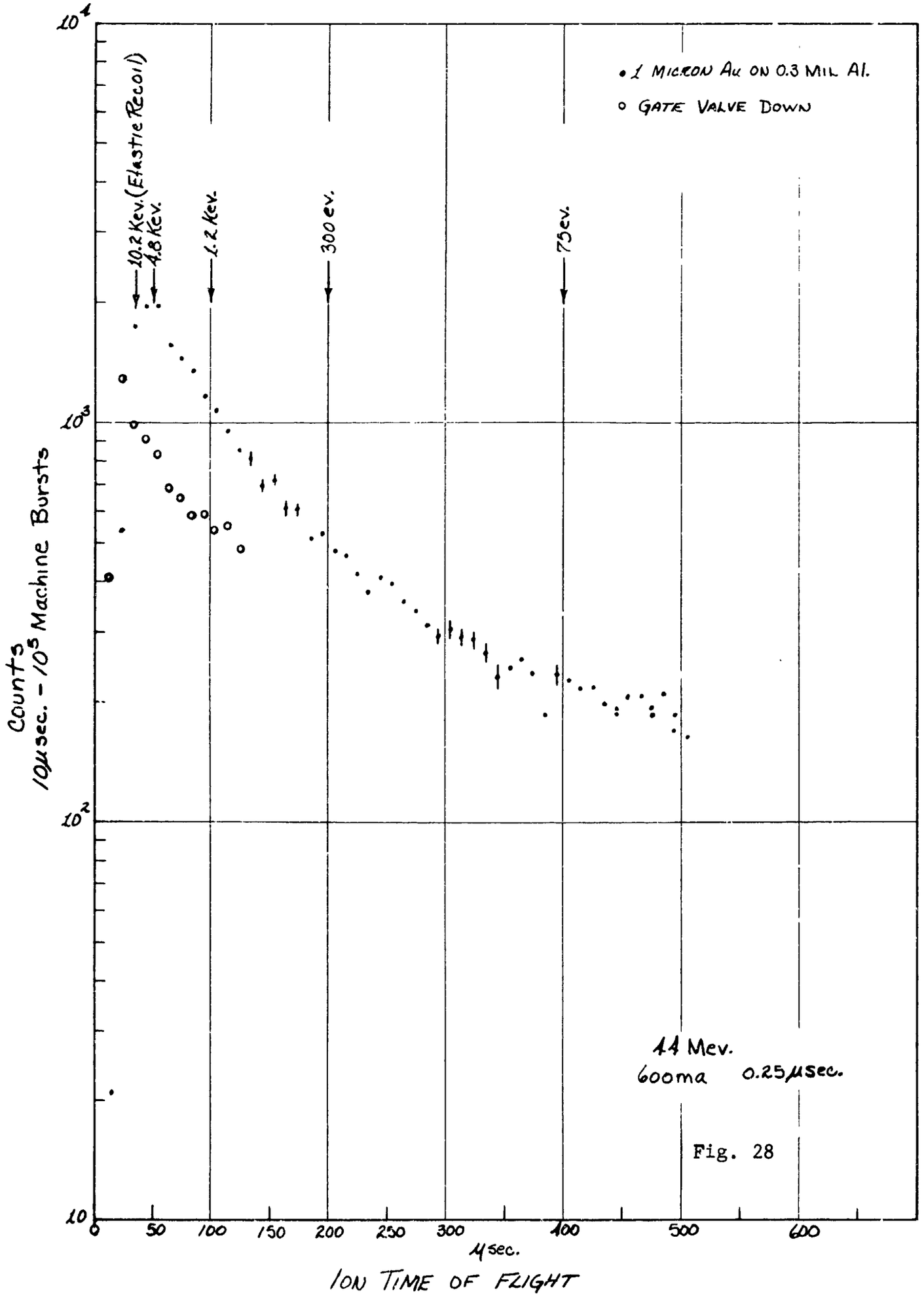
• 1 MICRON Au ON 0.3 MIL Al.
○ GATE VALVE DOWN
10.2 Kev. (Elastic Recoil)
4.8 Kev.
1.2 Kev.
300 ev.
75 ev.
Counts
10μsec. - 10⁵ Machine Bursts
10⁴
10³
10²
10
0
50
100
150
200
250
300
400
500
600
μsec.
ION TIME OF FLIGHT
14 Mev.
600ma 0.25μsec.

Fig. 28

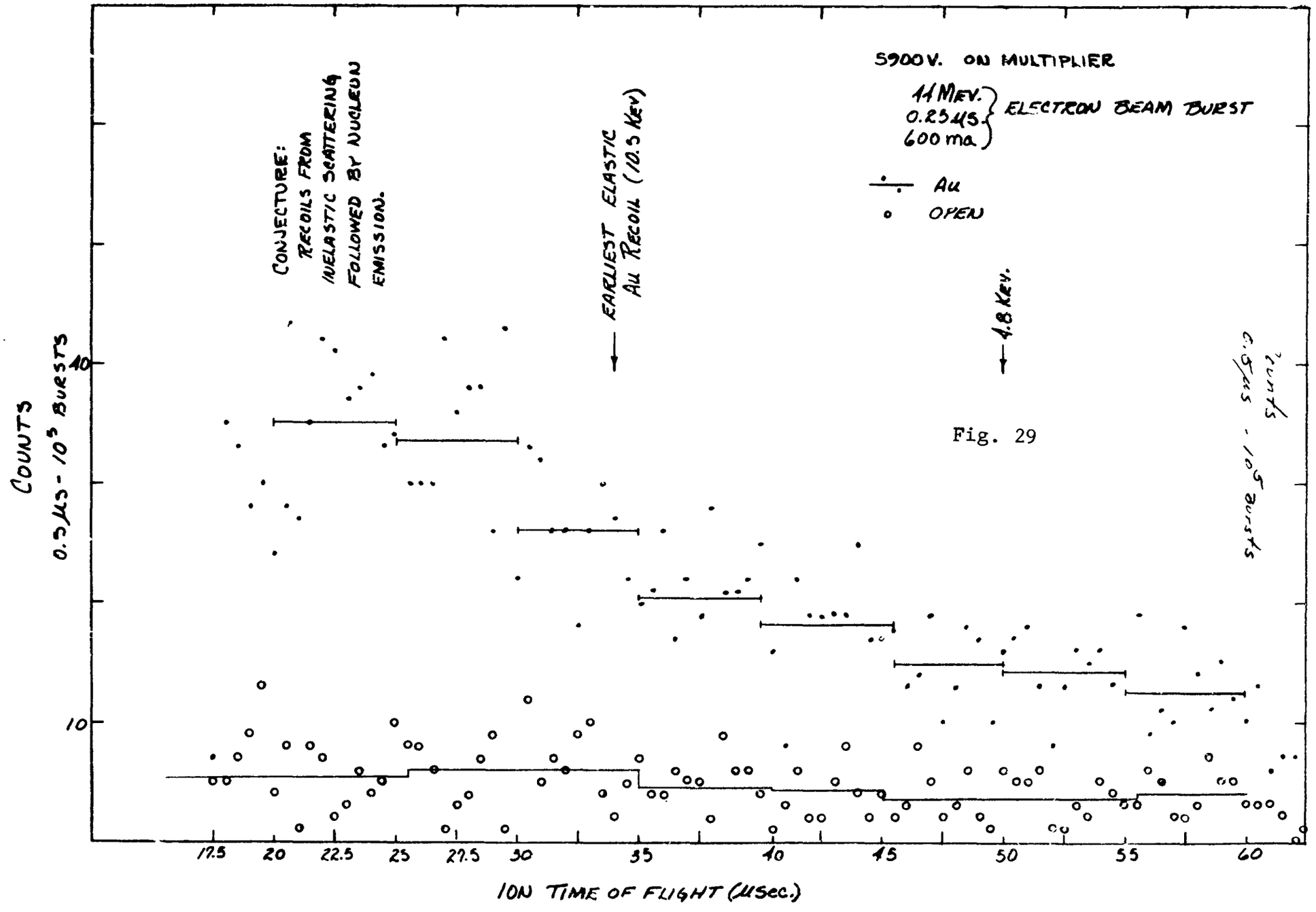
5900 V. ON MULTIPLIER
11 MEV.
0.25 μS
600 ma
ELECTRON BEAM BURST
Au
OPEN
CONJECTURE:
RECOILS FROM
INELASTIC SCATTERING
FOLLOWED BY NUCLEON
EMISSION.
EARLIEST ELASTIC
Au RECOIL (10.5 KEV)
4.8 KEV.
COUNTS
0.5 μS - 10³ BURSTS
10
40
17.5
20
22.5
25
27.5
30
35
40
45
50
55
60
ION TIME OF FLIGHT (μSec.)

Fig. 29

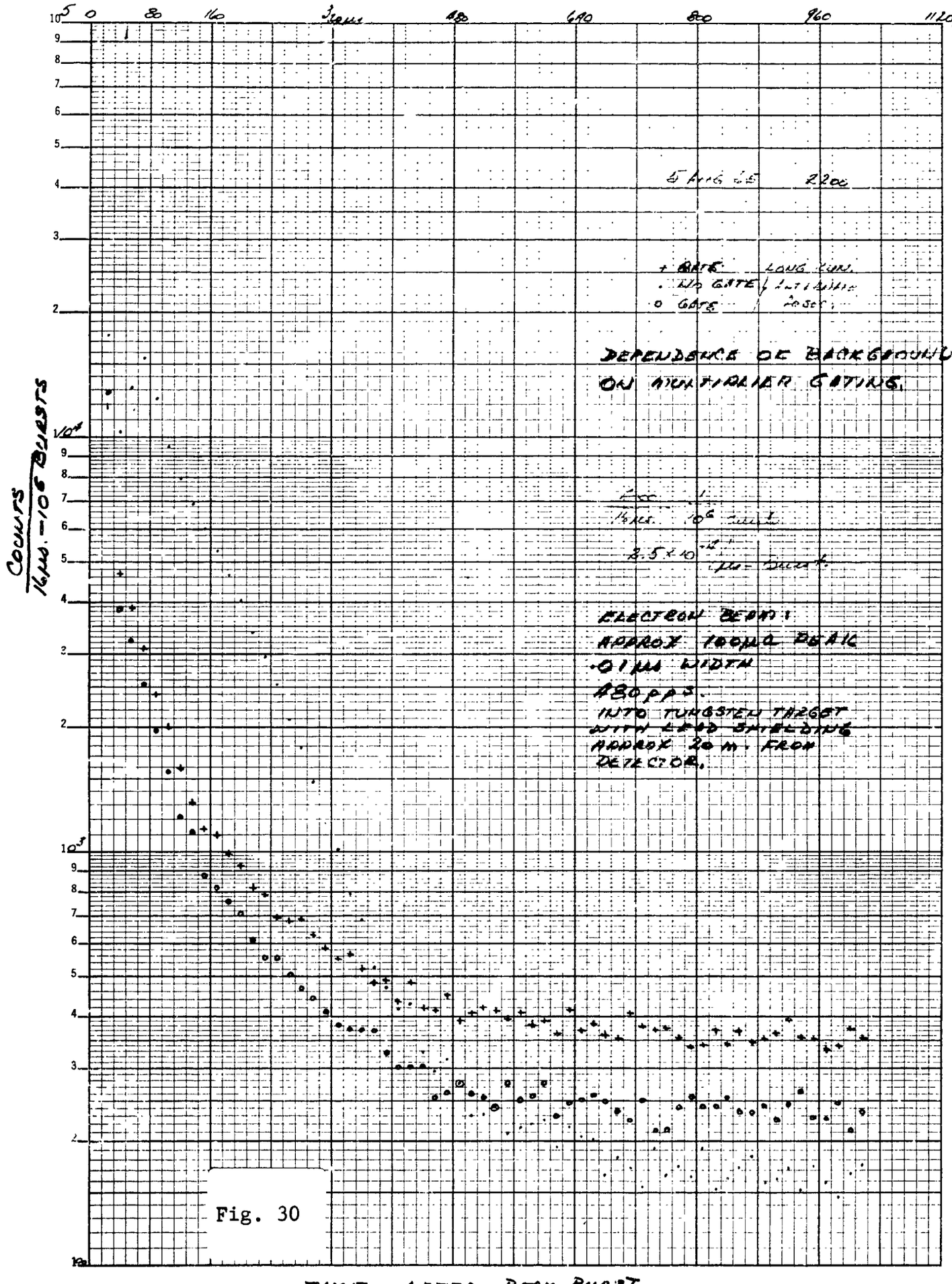
Counts / Kus. - 10⁶ Bursts
TIME AFTER BEAM BURST
DEPENDENCE OF BACKGROUND ON MULTIPLIER GATING.
ELECTRON BEAM:
APPROX 100MA PEAK
.01μs WIDTH
480 pps.
INTO TUNGSTEN TARGET
WITH LEAD SHIELDING
APPROX 20 m. FROM
DETECTOR.

Fig. 30

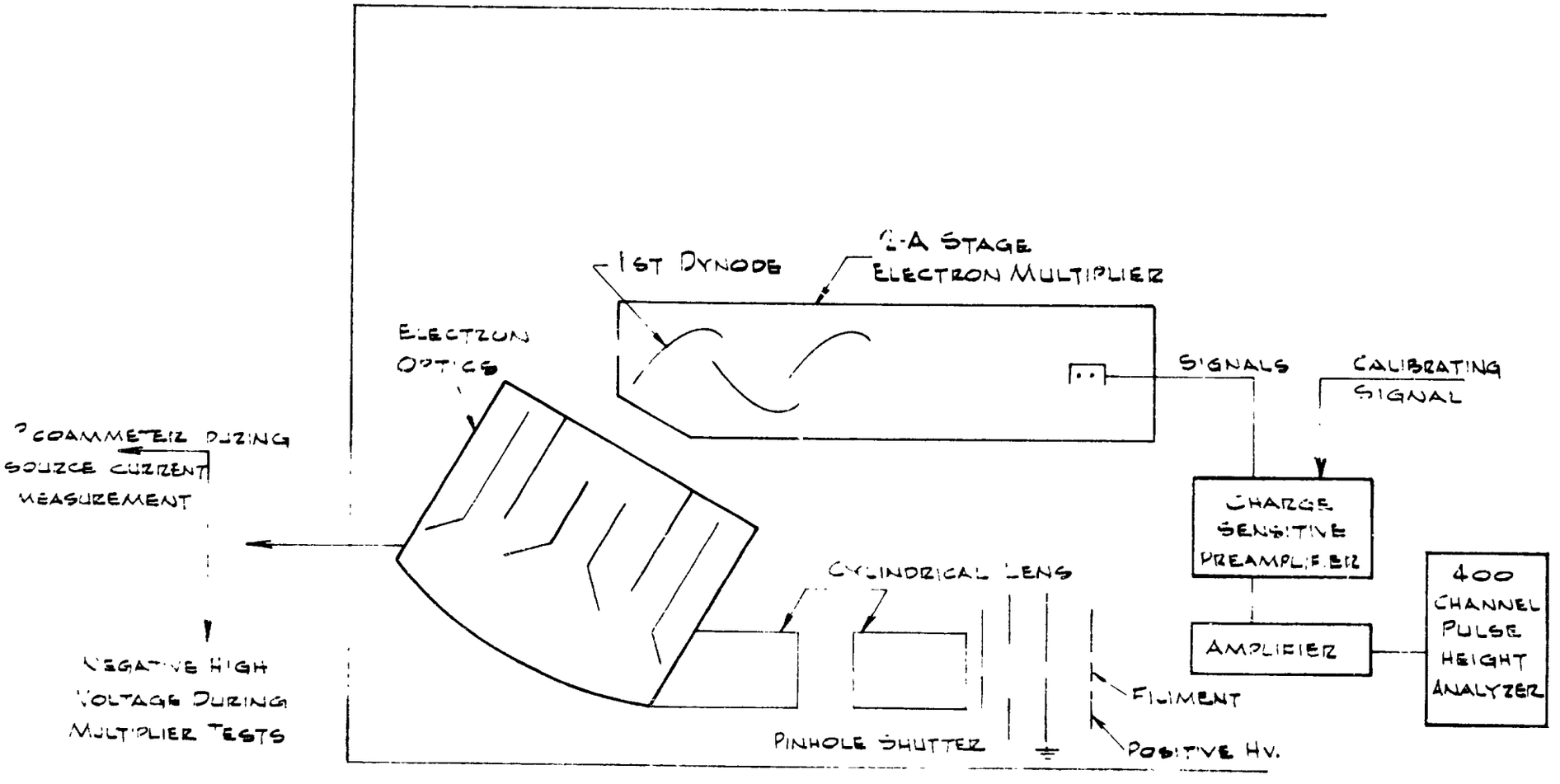

SCHEMATIC FOR
DETECTOR BENCH TESTS

Fig. 31

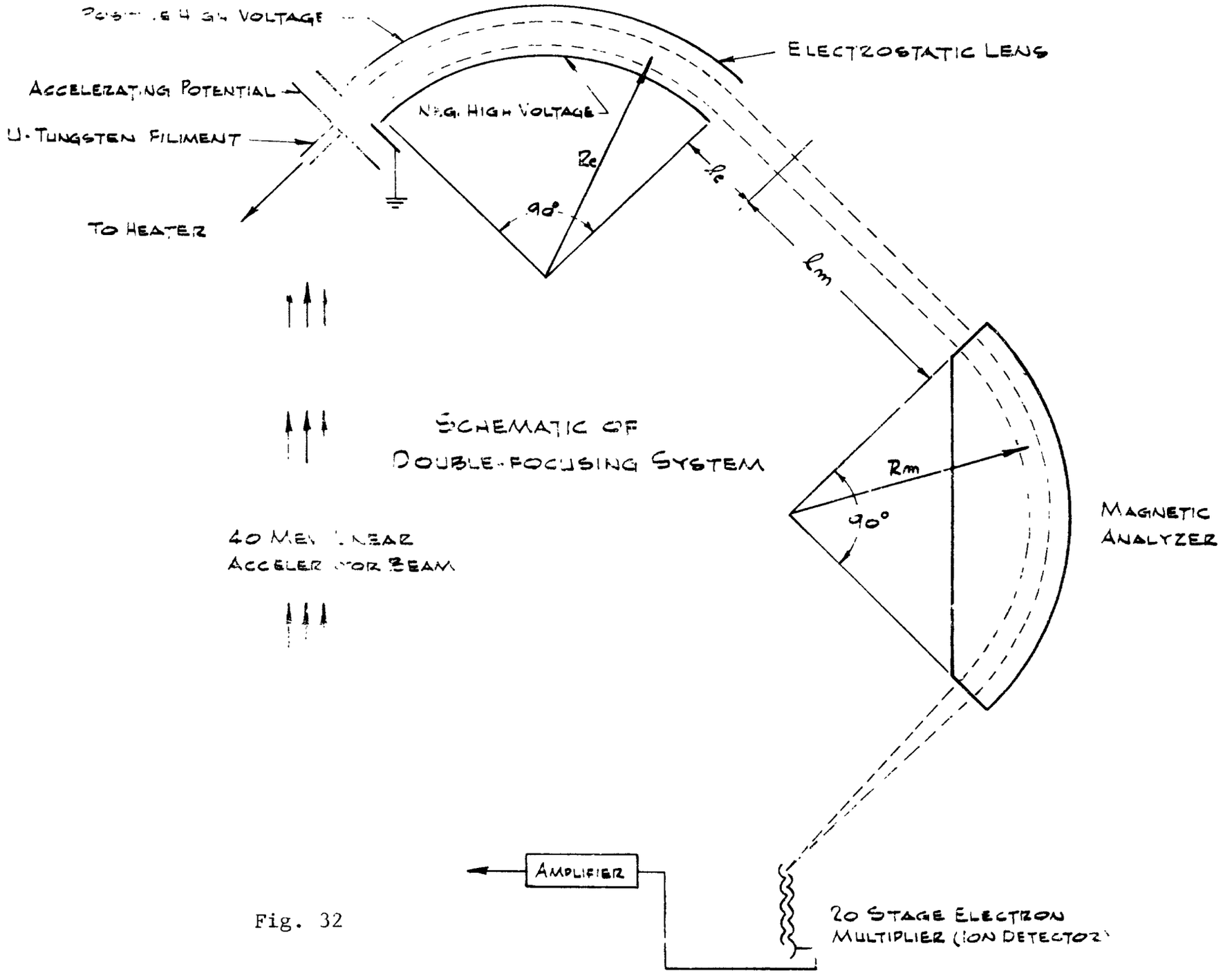

Schematic of Double-focusing System

40 Mev Linear Accelerator Beam

Fig. 32

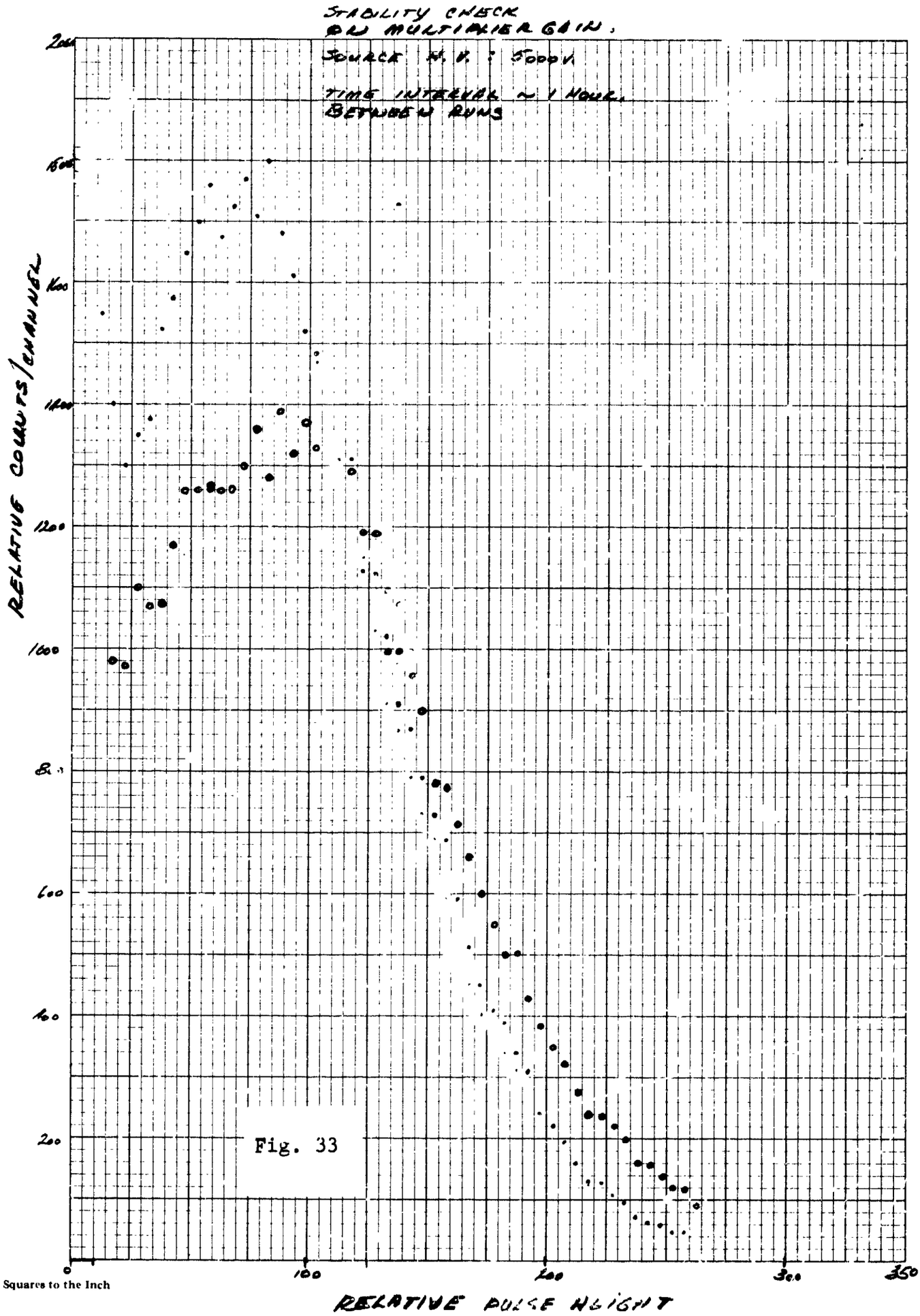

Fig. 33

10 Squares to the Inch